ASSESSMENT OF THE EFFECTIVENESS OF THE EMBEDDED THROUGH-SECTION TECHNIQUE FOR THE SHEAR STRENGTHENING OF RC BEAMS

J. A. O. Barros[1] and G. M. Dalfré[2]

[1] Full Prof., ISISE, Dep. of Civil Eng., Univ. of Minho, Azurém, 4810-058 Guimarães, Portugal

[2] PhD Candidate, ISISE, Dep. of Civil Eng., Univ. of Minho, Azurém, 4810-058 Guimarães, Portugal

Abstract

Embedded Through-Section (ETS) technique is a relatively recent shear strengthening strategy for reinforced concrete (RC) beams, and consists on opening holes across the depth of the beam's cross section, with the desired inclinations, where bars are introduced and are bonded to the concrete substrate with adhesive materials. To assess the effectiveness of this technique, a comprehensive experimental program composed of 14 RC beams was carried out, and the obtained results confirm the feasibility of the ETS method and revealed that: (i) inclined ETS strengthening bars were more effective than vertical ETS bars, and the shear capacity of the beams has increased with the decrease of the spacing between bars; (ii) brittle shear failure was converted in ductile flexural failure, and (iii) the contribution of the ETS strengthening bars for the beam shear resistance was limited by the concrete crushing or due to the yielding of the longitudinal reinforcement. The applicability of the ACI 318 (2008) and Eurocode 2 (2004) standard specifications for shear resistance was examined and a good agreement between the experimental and analytical results was obtained.

1. Introduction

This paper reports the relevant results obtained from an experimental program carried out to assess the effectiveness of the Embedded Through-Section (ETS) technique for the shear strengthening of RC beams. The ETS shear strengthening concept is schematically represented in Figure 1. According to the this technique, holes are opened across the thickness of the beam's cross section, with the desired inclinations, and steel or FRP bars are introduced into these holes and bonded to the concrete substrate with adhesive materials. Since the strengthening

[1] Author to whom the correspondence should be sent (barros@civil.uminho.pt).

bars are inserted into holes open through the cross section, they are much better protected from fire, and from the influence of environmental aggressive agents and vandalism acts than externally bonded reinforcement (EBR) and near surface mounted (NSM) techniques based on the use of fibre reinforced polymer (FRP) systems (Barros *et al.*, 2007; Dias and Barros, 2012). This research program has started in 2007, where the use of FRP and steel bars, applied according to a technique that was originally designated by Core Drilled Mounted (CDM), was explored for the shear strengthening of concrete elements. In this context, direct shear tests were executed with the purpose of capturing the main features of FRP/Steel CDM bars for the shear resistance, and to provide data for a rational decision about the most effective bars and adhesives for this type of application (Barros et al., 2008). From the results, a significant increase in shear strength was obtained with a relatively low reinforcement ratio, and it was verified that steel bars were very effective. By using the obtained results it was verified that closed form solution developed by Bianco *et al.* (2009) is capable of simulating with reasonable accuracy the bond behaviour recorded in that tests (Trombini, 2008). In a second phase of this project, a program of pullout tests with steel bars was carried out, where the influences on the bond phenomena of the following parameters were assessed (Dalfré *et al.*, 2011): type of adhesive; thickness of the adhesive layer (2, 4, 5 and 6 mm); diameter of the steel bar; bond length (50 and 75 mm) . It was found that the type of adopted adhesives has a significant influence on the bond behaviour. The results also evidenced that for the values adopted for the anchorage length and for the adhesive layer thickness, the bond strength is marginal affected, but this last property has increased with the Young's modulus of the adhesive.

In this context, the present paper resumes the research of the third part of this project, where the effectiveness of the ETS shear strengthening technique is assessed. For this purpose, an experimental program composed of two series of RC beams of different cross section was carried out. The variables examined in this experimental program were: (i) spacing of existing steel stirrups (225 and 300 mm), (ii) inclination of the strengthening steel bars with respect to the longitudinal axis of the beam (vertical and 45-degrees), and (iii) interaction of existing steel stirrups and the strengthening bars.

Limited research has been conducted on the use of embedded bars for the shear strengthening. Valerio *et al.* (2005, 2009) performed some tests on unstrengthened and ETS strengthened beams. They also executed pull-out tests on carbon, glass, aramid and steel bars embedded into concrete with different embedment lengths (15, 30, 45, 60 and 75 mm) and adhesive materials in order to assess the bond properties and select the most suitable strengthening bars for the ETS technique. These pull-out tests have shown that the ETS strengthening effectiveness relies on the bond between the embedded bar and the surrounding concrete, and also evidenced that the bond–slip response of the system is ductile when appropriate adhesives and bars with proper surface are used. Concerning the beams strengthened with ETS FRP bars, a strengthening ratio of 0.24%, 0.36% and 0.48% has conducted to an increase of load carrying capacity of, respectively, 33%, 42% and 84% with respect to the reference beam.

Chaalal *et al.* (2011) carried out some tests to assess the effectiveness of the ETS FRP technique, and to compare the performance of ETS, EBR and NSM methods. The results shown that the techniques based on the use of EBR U-jacket sheet, NSM FRP rods, and ETS FRP rods have provided an average increase in shear capacity of, respectively, 23%, 31% and 60%. Additionally, the ETS technique was more efficient in terms of mobilizing the tensile capacity of FRP systems, since they have failed due to the attainment of their tensile strength when applied according to the ETS technique, while the EBR systems failed by debonding, and the NSM rods by the separation of the concrete cover. At the failure of the FRP systems applied according to the EBR and NSM techniques, the maximum tensile strain was much lower than their ultimate tensile strain.

In the present paper the experimental research carried out is described and the obtained results are presented and analyzed. Additionally, the ACI and Eurocode 2 analytical formulations, proposed for the prediction of the shear resistance of FRP-based shear strengthened RC beams, are applied to the ETS shear strengthened beams, and their predictive performance is assessed.

2. Experimental program

2.1 Specimens

The experimental program is formed by two series, A and B, composed of beams with a cross section of 150x300 mm^2 and 300x300mm^2, respectively, with a total length of 2450 mm and a shear span length of 900 mm (Figures 2 to 4, and Table 1). The longitudinal tensile steel reinforcement of A and B series consists of two and three steel bars of 25 mm diameter (∅ 25 mm), respectively. The longitudinal compressive steel reinforcement was composed of two and three steel bars of 12 mm diameter (∅ 12 mm) in the A and B series, respectively. Steel stirrups of two vertical arms and 6 mm diameter were used. The concrete clear cover for the top, bottom and lateral faces of the beams was 20 mm.

Each series is made up of a beam without any shear reinforcement (reference beam) and a beam for each of the following shear reinforcing systems: (i) steel stirrups of ∅6 mm at a spacing of 300 mm, (ii) ETS strengthening bars at 45º or at 90º in relation to the beam axis, with a spacing of 300 mm, (iii) steel stirrups of ∅6 mm at a spacing of 300 mm and ETS strengthening bars at 45º or at 90º with a spacing of 300 mm. Additionally, for the A Series, two other shear reinforcing systems were also tested: (iv) steel stirrups of ∅6 mm at a spacing of 225 mm and (v) steel stirrups of ∅6 mm at a spacing of 225 mm and ETS strengthening bars at 90º with a spacing of 225 mm. For the series A and B, ETS bars of ∅10 mm and ∅8 mm were used, respectively. It should be noted that an ETS bar was designed as a stirrup of one arm, following the design recommendations of ACI Code (2008) for the steel stirrups in the context of shear reinforcement or RC beams.

Table 1 includes general information of the beams composing the two series, where ρ_{sl} is the longitudinal steel reinforcement ratio [$\rho_{sl} = (A_{sl}/b_w \cdot d)\times 100$, where A_{sl} is the cross sectional area of the longitudinal steel bars, b_w is the web width and d is the distance from the extreme compression fibre of the cross section to the centroid of the longitudinal reinforcement]. In Table 1, the shear reinforcement ratio (ρ_{sw}) is obtained from $\rho_{sw} = (A_{sw}/b_w \cdot s_w)\times 100$, where A_{sw} is the cross sectional area of the two arms of a steel stirrup, and s_w is the spacing between stirrups. Finally, the ρ_{fw} indicated in Table 1 is the ETS strengthening ratio defined by $\rho_{fw} = A_f/(b_w \cdot s_f \cdot sin\theta_f)\times 100$, where A_f is the cross sectional area of a ETS shear strengthening bar, s_f is the spacing between these bars and θ_f is the inclination of the strengthening bars with respect to the longitudinal axis of the beam. The number of days between the strengthening intervention and the test is indicated in Table 1. Since the beams were not cast in the same batch, the corresponding batch is also indicated in this Table.

2.2 Test setup and monitoring system

Figure 5 depicts the positioning of the sensors for data acquisition. To measure the deflection of a beam, four linear voltage differential transducers (LVDTs) were supported in a suspension yoke (see Figure 5a). The LVDT 3558 was also used to control the test at a displacement rate of 20 μm/s up to the failure of the beams. The beams were loaded under three-point bending configuration with a shear span (a) of 900 mm, which corresponds to a a/d ratio of 3.44, where d is the depth of the longitudinal reinforcement (Figure 2). The applied load (F) was measured using a load cell of ±500 kN and accuracy of ±0.05%. Two or three electrical resistance strain gauges (S1 to S3), depending on the shear reinforcement arrangement, were installed in the steel stirrups to measure the strains. Additionally, six or eight SGs (1 to 8) were bonded on the ETS strengthening bars according to the strengthening arrangement represented in Figure 5b.

2.3 Material properties

Table 2 includes the values obtained from the experimental tests for the characterization of the main properties of the materials used in the present work. The average compressive strength (f_{cm}) was determined according to NP-E397 (1993). To characterize the tensile behaviour of the steel bars, uniaxial tensile tests were conducted according to the standard procedures of ASTM 370 (2002). Sikadur 32N structural epoxy bonding agent was used to bond the ETS steel bars to the concrete. For the characterization of the tensile behaviour of this adhesive, uniaxial tensile tests were performed according to the procedures outlined in ISO 527-2 (1993).

2.4 Strengthening technique steps

The ETS shear strengthening technique is represented in Figure 6. Before drilling the holes, a rebar detector was used to verify the position of the existing longitudinal bars and stirrups. Afterward, the positions of the strengthening bars were marked on the RC beams, and holes were made with the desired inclination through the core of the cross-section of the RC beams. These holes had 16 mm or 18 mm of diameter, where bars of 8 mm or 10 mm diameter were introduced, respectively, resulting in an adhesive layer of about 4 mm thickness. The holes were cleaned with compressed air, and one extremity of the holes was blocked before bonding the strengthening bars to the concrete. The bars were cleaned with acetone to remove any possible dirt. The adhesive was prepared according to the supplier recommendations, and the bars were introduced into the holes that were filled with the adhesive (care was taken to prevent air bubble formation in the adhesive layer during the application of the strengthening system). Finally, the adhesive in excess was removed. A period of 15 days was dedicated to cure the adhesive (in laboratory environmental conditions) prior to testing the beams.

2.5 Main results

Figures 7a and 7b show the relationship between the total applied load and the deflection of the loaded section, *F-u*, of the beams of A and B Series, respectively. Two phases occurred during each test in the following sequence: 1st) the reference and the strengthened beams show similar response up to the formation of the shear failure crack in the reference beam; 2nd) after the shear crack initiation, the stirrups and/or the strengthening bars were effectively activated, as can be shown from the load-strain diagrams represented in Figures 9 to 12 and 14 to 16, which has provided an increase of load carrying and deflection capacity, whose level depends on the shear reinforcement arrangements. In fact, the ETS bars have started to strain at an applied load of approximately 90 kN and 200 kN for the A and B Series, respectively.

For similar ρ_{sw} and ρ_{fw} the RC beams reinforced with steel stirrups or strengthened with ETS bars have identical behaviour (S300.90 and E300.90 beams). For the beams with ETS bars of equal spacing but different inclination (which means different shear strengthening ratio, ρ_{fw}), ETS bars applied at 45-degrees have provided a higher increase in terms of load carrying capacity and deflection at peak load (E300.90 versus E300.45 beams of both series). In series B, similar stiffness was observed in all beams up to their peak load, which indicate a prevalent influence of the concrete aggregate interlock for the stiffness due to the larger width of the cross section of the beams of this series. Due to the significant increase in the shear capacity provided by the ETS bars, the beams reinforced with steel stirrups and strengthened with ETS bars collapsed by the yielding of the longitudinal steel bars, followed by concrete crushing. In the design phase of the ETS strengthening systems it was not expected a so high shear strengthening effectiveness for these systems. If a higher ρ_{sl} was adopted, from the theoretical point of view the increase level of the ultimate load would have been even higher than the ones registered in the present experimental program, as long as the concrete crushing could be avoided. However, for the geometry and concrete compressive strength of the beams adopted in this experimental program the ρ_{sl} was designed in order to occur concrete crushing just after yield initiation of the longitudinal reinforcement, as recommended by good design practice of RC elements.

Table 3 presents the main results obtained in the experimental tests. In this Table, $F_{\max}$ is the maximum value of the load registered in the load cell during the test, $\Delta F_{\max} / F_{\max}^{REF}$ is the ratio between the increase in terms of load carrying capacity provided by the shear reinforcing system, $\Delta F_{\max}$, and the maximum load supported by the reference beam, $F_{\max}^{REF}$, $\delta_{F\max}$ is the deflection of the loaded section at $F_{\max}$, and $\Delta\delta_{F\max}/\delta_{F\max}^{REF}$ is the ratio between the increase in terms of deflection capacity provided by the shear reinforcing system, $\Delta\delta_{F\max}$, and the deflection at $F_{\max}^{REF}$, $\delta_{F\max}^{REF}$. Additionally, $V_n = 0.6F_{\max}$ is the shear resistance of the beam, and V_c, V_s and V_f are the shear resistance attributable to the concrete, steel stirrups and ETS strengthening bars, respectively ($V_n = V_c + V_s + V_f$). Finally, $\varepsilon_{s,F\max}$ and $\varepsilon_{f,F\max}$ are the maximum strains in the steel stirrups and in the ETS strengthening bars at $F_{\max}$, while $\varepsilon_{s,\max}$ and $\varepsilon_{f,\max}$ are the maximum strains in the stirrups and ETS bars up to the failure of the corresponding beams. Note that the values indicated in Table 3 were obtained based on the following assumptions: a) the shear resistance due to concrete is the same regardless the beam is reinforced with steel stirrups or/and strengthened with ETS bars; and b) the contribution of steel stirrups for the shear resistance is the same in strengthened and unstrengthened beams.

From the obtained results, included in Table 3, it can be pointed out the following main observations:

(i) The use of steel ETS bars for the shear strengthening provided significant increase of the load carrying capacity of RC beams for the both bar orientations considered. The effectiveness was also significant in terms of the deflection performance.

(ii) Based on the results of the unstrengthened beams (Reference), it was found that the beams reinforced with steel stirrups (S300.90) and the beam strengthened according to the ETS technique (E300.90) presented an increase in the load carrying capacity of 51 % and 48 % (A Series), and of 14 % and 17% (B Series), respectively. In terms of deflection capacity ($\delta_{F\max}$), an increase of 110 % and 74 % (A Series) and of 25 % and 36 % (B Series), respectively, was obtained.

(iii) The shear reinforcing system composed by inclined ETS strengthening bars was more effective than vertical ETS bars, having assured a better performance in terms of load and deflection capacities. This is justified by the orientation of the shear failure cracks that had a tendency to be almost orthogonal to inclined ETS bars. Furthermore, for vertical ETS bars, the total resisting bond length is lower than that of inclined ETS bars, and ρ_f of vertical ETS bars is lower than ρ_{fw} of inclined ETS bars for the same spacing. Based on the results of the E300.90 beams, it was found that the E300.45 beams presented an increase in the load carrying capacity of 27 % and 41% for A and B Series, respectively. The deflection capacity has also increased in 72 % and 55 % for A and B Series, respectively.

(iv) Since the strains recorded by strain gauges (SGs) are quite dependent of the relative position between the SGs and the shear failure crack, remarks based on these values should not be regarded as conclusions. However, since ETS shear strengthening systems have increased significantly the load carrying capacity of the RC beams, the increase of the maximum strains in both stirrups and ETS bars was expected, and, in general, they have exceeded the yield strain of the stirrups and ETS bars. The maximum strain in the ETS bars, $\varepsilon_{f,\max}$, was particularly high when positioned at 45-degrees.

2.6 Analysis of the beams of A series (150x300 mm^2 cross section)

2.6.1 Reference beam

Figure 8 represents the total load versus the deflection, $F-u$, registered in the LVDTs of the A.1 beam, as well as the schematic representation of the crack pattern at failure. During loading of A.1 reference beam, visible diagonal shear cracks formed at a load of 42 kN. With the increase of the load the shear failure crack has widen and an abrupt failure has occurred at a load of 108.86 kN. The maximum deflection recorded in the loaded section was equal to 4.01 mm. After the development of a reduced number of flexural cracks, this beam has failed by the occurrence of a unique shear crack at the smaller shear span (a).

2.6.2 Beams with steel stirrups

Figure 9a represents the $F-u$ registered in the LVDTs of the A.2 beam, as well as the schematic representation of the crack pattern at failure. In the A.2 and A.7 beams, a brittle shear failure has occurred at a maximum load ($F_{\max}$) of 164.67 kN and 180.31 kN, respectively, which correspond to an increase of 51.27% and 65.63% with respect to the carrying capacity of the A.1 reference beam. At first, flexural cracks were formed near the loaded section, and with the increase of the load other flexural cracks have propagated along the shear span. Some of these flexural cracks have degenerated in shear cracks during the subsequent loading stages. Finally, the beams have abruptly failed with the formation of a shear crack at the shear span (Figure 17). In the beam with stirrups at a spacing of 300 mm (A.2), the first visible crack was formed at a load of 77 kN. In Figure 9c is represented the load versus the strains recorded in the strain gauges (SG) installed in the stirrups, $F-\varepsilon_s$, (see also Table 3).The maximum strain in the stirrups, $\varepsilon_{s,\max}$, was recorded in the S2 strain gauge (SG), in the second stirrup, at 600 mm from the applied load (Figure 4), close to the zone crossed by the diagonal crack, and was approximately equal to 2953 με, indicating that this stirrup has yielded (Table 3).

Figure 9b represents the $F-u$ registered in the LVDTs of the A.7 beam, as well as the schematic representation of the crack pattern at failure. In this beam, the first visible crack was formed at a load of 37 kN. The $F-\varepsilon_s$ of the stirrups of A7 beam is represented in Figure 9d. The maximum strain was recorded in the S2 SG of stirrup number 2 (450 mm from the applied load) and was equal to 4555 με. It must be pointed out that these strain values and all those reported herein are not necessarily the maximum values installed in the stirrups and ETS bars. They only represent the strains in the regions where the strain gauges are bonded. The A.2 and A.7 beams presented a deflection of 8.40 mm and 9.92 mm at $F_{\max}$ ($\delta_{,F\max}$), respectively, which corresponds to an increase of 109.47% and 147.38% with respect to the reference beam.

Figure 17 shows that the first stirrup from the support has ruptured in A.2 beam, while in the A.7 beam the first two stirrups from the support have ruptured.

2.6.3 Beams without steel stirrups and strengthened according to the ETS technique

Two different inclinations of the ETS bars with respect to the longitudinal axis of the beams were used, vertical (A.3 beam) and at 45-degrees (A.4), maintaining the same spacing between bars (300 mm). Figure 10a represents the $F-u$ registered in the LVDTs of the A.3 beam, as well as the schematic representation of the crack pattern at failure. In the A.3 beam, the first visible crack was registered at a load of 36 kN. The maximum load of 160.78 kN was attained at a deflection of 6.97 mm. In Figure 10c is represented the load versus the strains recorded in the strain gauges (SG) installed in the ETS bars of A.3 beam, $F-\varepsilon_f$ (see also Table 3). The maximum strain was recorded in the SG 3 installed in the ETS bar number 3 (450 mm from the applied load) and was equal to 8379 με.

Figure 10b represents the $F-u$ registered in the LVDTs of the A.4 beam, as well as the schematic representation of the crack pattern at failure. The A.4 beam has presented a maximum load of 203.98 kN for a deflection of 12.04 mm. The first visible crack was registered at a load of 38 kN. The $F-\varepsilon_f$ of the ETS bars of A4 beam is represented in Figure 10d. The maximum strain was recorded in the SG 4 placed in the ETS bar 4 (600 mm from the applied load) and was equal to 4124 με.

Figure 17 shows that in the A.3 beam the stirrups have not ruptured and two shear cracks were formed. In A.4 beam two shear failure cracks were also formed, but involved with a much diffuse crack pattern.

The analysis of the obtained results prompts the following conclusions:

i) The maximum carrying capacity of the beam strengthened with vertical ETS bars (A.3) was almost the same of the beam with steel stirrups (A.2). Moreover, a reduction on the $\delta_{,F\max}$ of about 17% was observed in the strengthened beams.

ii) The beams strengthened with ETS bars at 45-degrees (A.4) presented an increase of 23.87% and 43.33% in terms of $F_{\max}$ and $\delta_{,F\max}$, respectively, when the beam reinforced with steel stirrups (A.2) is taken for comparison purposes. When compared to the A.3 beam, the A.4 beam presented an increase of 26.87% and 72.74% in terms of $F_{\max}$ and $\delta_{,F\max}$, respectively. The more ductile response of A.4 beam, when compared to A.2 and A.3, is evident in Figure 7.

2.6.4 Beams with steel stirrups and strengthened according to the ETS technique

Three beams were strengthened according to different arrangements of stirrups and ETS bars in order to assess the ETS shear strengthening effectiveness for distinct percentages of existing stirrups, and to evaluate the influence of the percentage and inclination of ETS bars on this effectiveness. Two of these beams were strengthened with steel stirrups and ETS bars at a spacing of 300 mm, one with vertical ETS bars (A.5), and the other at 45-degrees (A.6). The third beam (A.8) was strengthened with stirrups and vertical ETS bars at a spacing of 225 mm.

Figures 11a and 11b represent the $F-u$ registered in the LVDTs of the A.5 and A.6 beams, as well as the schematic representation of the crack pattern at failure. When using vertical stirrups at a spacing of 300 mm, failure occurred at a load of 231.83 kN and 244.41 kN for the A.5 and A.6 beams, respectively, which correspond to an increase of 40.78% and 48.42% with respect to the load carrying capacity of the beam shear strengthened only with steel stirrups at a spacing of 300 mm (A.2). In terms of deflection capacity, the A.5 and A.6 beams presented a deflection of 13.12 mm and 14.00 mm at $F_{\max}$, corresponding to an increase of 56.19% and 66.67% with respect to the beam with steel stirrups at a spacing of 300 mm (A.2).

In the beam strengthened with vertical ETS bars (A.5) the first visible crack was registered at a load of 58 kN. In Figure 11c is represented the $F-\varepsilon_s$ recorded in the SG installed in the stirrups of A.5 beam, while the $F-\varepsilon_f$ registered in the SG applied in the ETS bars of this beam is shown in Figure 11e.The maximum strain was recorded in the stirrup number 2 (600 mm from the applied load) and was equal to 3080 με. In this beam the maximum strain in ETS bars was recorded in the SG 1 (150 mm from the applied load) and was equal to 2683 με.

In the beam strengthened with 45-degree ETS bars (A.6), the first visible crack was registered at a load of 30 kN. In Figures 11d and 11f are represented the $F-\varepsilon_s$ and $F-\varepsilon_f$ for beam A.6. The maximum strain was recorded in the stirrup number 1 (300 mm from the applied load) and was equal to 2696 με. The maximum strain in the ETS bars was recorded in the SG 4 and was equal to 17297 με.

Figure 12a represents the $F-u$ registered in the LVDTs of the beam reinforced with vertical stirrups and strengthened with vertical ETS bars at a spacing of 225 mm (A.8). The schematic representation of the crack pattern at failure is also illustrated. In this beam, the first visible crack was formed at a load of 28 kN. This beam reached a maximum load of 244.17 kN, which corresponds to an increase of 35.42% with respect to the load carrying capacity of the beam with steel stirrups at a spacing of 225 mm (A.7). In Figure 12b is represented the $F-\varepsilon_s$ recorded in the SG installed in the stirrups of A.8 beam, while the $F-\varepsilon_f$ registered in the SG applied in the ETS bars of this beam is shown in Figure 12c. The maximum strain was recorded in the SG 2 on the stirrup number 3 (675 mm from the applied load), which was equal to 2309 με. The maximum strain in the vertical ETS bars was recorded in the SG 5 (562.50 mm from the applied load) and was equal to 4695 με. The A.8 beam presented a deflection of 14.44 mm at $F_{\max}$, which corresponds to an increase of 45.56% with respect to the deflection capacity of the beam with steel stirrups at a spacing of 225 mm (A.7).

Figure 17 shows that in the A.5 and A.6 beams a quite diffuse crack pattern was formed. In A.5 beam the intermediate stirrup, which was crossed by the widened shear crack, has ruptured.

2.7 Analysis of the beams of B series (300x300 mm^2 cross section)

2.7.1 Reference Beam

Figure 13 represents the total load versus the deflection, $F-u$, registered in the LVDTS of the B.1 beam. The schematic representation of the crack pattern at failure is also illustrated. The crack pattern during the loading process of this beam (B.1) was similar to the A.1 beam, but due to the larger width of the cross section the maximum shear failure load ($F_{\max}$) was higher, equal to 203.36 kN. At $F_{\max}$ the deflection recorded under the applied load was equal to 4.45 mm, a little bit greater than the value measured in A.1 beam. As Figure 17 shows, the crack pattern of B.1 beam was quite similar to the one registered in A.1 beam.

2.7.2 Beams with steel stirrups

Figure 14a represents the $F-u$ registered in the LVDTs of the B.2 beam. The schematic representation of the crack pattern at failure is also included in this figure. In the B.2 beam with vertical stirrups at a spacing of 300 mm a brittle shear failure has also occurred at a $F_{\max}$ of 232.31 kN, corresponding to an increase of 14.24 % with respect to the $F_{\max}$ of the B.1 reference beam. The crack propagation process during the loading process was similar to the one of the homologous beam of A series (A.2).

In the B.2 beam with stirrups at a spacing of 300 mm, the first visible crack was formed at a load of 47 kN. In Figure 14b is represented the load versus the strains recorded in the strain gauges (SG) installed in the stirrups, $F-\varepsilon_s$, (see also Table 3). Such in the homologous A.2 beam of series A, the maximum strain in the stirrups was recorded in the S2 strain gage, which is positioned close to the zone crossed by the diagonal crack, and a strain of 18696 με was measured. This B.2 beam presented a deflection of 5.56 mm at $F_{\max}$, which corresponds to an increase of 24.94 % with respect to the deflection capacity of the B.1 reference beam, but it is smaller than the deflection registered in A.2 beam.

Figure 17 shows that, like in the A.2 beam, in the B.2 beam the first stirrup from the support has ruptured, however, the in-plane shear crack formed just above the longitudinal bars in the A.2 beam (parallel to the longitudinal reinforcement) has not occurred in the B.2 beam.

2.7.3 Beams without steel stirrups and strengthened according to the ETS technique

Figure 15a represents the $F-u$ registered in the LVDTs of the B.3 beam strengthened with vertical ETS bars. The schematic representation of the crack pattern at failure is also illustrated. In this beam, the first visible crack was registered at a load of 54 kN. The maximum load of 238.88 kN was attained at a deflection of 6.06 mm. In Figure 15c is represented the load versus the strains recorded in the strain gauges (SG) installed in the ETS bars of B.3 beam, $F-\varepsilon_f$ (see also Table 3). The maximum strain was recorded in the SG 4 installed in the ETS bar 4 at 450 mm from the applied load, which was equal to 1133 με.

Figure 15b represents the $F-u$ registered in the LVDTs of the B.4 beam strengthened with ETS bars at 45-degrees. The schematic representation of the crack pattern at failure is also included.The first visible crack in the B.4 beam was registered at a load of 69 kN. This beam presented a maximum load of 336.19 kN at a deflection of 9.42 mm. The $F-\varepsilon_f$ of the ETS bars of A4 beam is represented in Figure 15d. The maximum strain was recorded in the SG 4 installed in the ETS bars from 300 mm of the applied load, and was equal to 3200 με.

As Figure 17 shows, the failure crack patterns of B.3 and B.4 beams were similar to those registered in the A.3 and A.4 beams.

The analysis of the obtained results prompts the following conclusions:

i) The B.3 beam strengthened with vertical ETS bars presented a load carrying capacity and a deflection performance that was 2.83 % and 9.00 % higher than the corresponding values registered in the B.2 beam reinforced with stirrups.

ii) When also compared to the B.2 beam, the B.4 beam strengthened with ETS bars at 45-degrees presented an increase of 44.72% and 69.42% for the load carrying and deflection capacity, respectively.

iii) A comparison between B.4 and B.3 beams reveals that applying ETS bars at 45 degrees conducted to an increase of 40.74 % on the load carrying capacity and an increase of 55.44 % on the deflection performance.

2.7.4 Beams with conventional steel stirrups and strengthened according to the ETS technique

Figures 16a and 16b represent the $F-u$ registered in the LVDTS of the B.5 and B.6 beams. The schematic representation of the crack pattern at failure is also illustrated in these figures. The failure of the beam with vertical (B.5) and 45-degrees ETS bars (B.6) occurred at a load of 390.11 kN and 396.51 kN, respectively, which correspond to an increase of 67.93% and 70.68% with respect to the carrying capacity of the B.2 beam with steel stirrups at a spacing of 300 mm. The deflection at $F_{\max}$ of B.5 and B.6 beams was 15.01 mm and 20.18 mm, which corresponds to an increase of 169.96 % and 262.95 % with respect to the deflection capacity of B.2 beam. In the B.5 beam, the first visible crack was registered at a load of 58 kN. In Figure 16c is represented the $F-\varepsilon_s$ recorded in the SG installed in the stirrups of B.5 beam, while the $F-\varepsilon_f$ registered in the SG applied in the ETS bars of this beam is shown in Figure 16e. The maximum strain was recorded in the SG 2 of the stirrup at 600 mm from the applied load and was equal to 3267 με, while in the ETS bars a maximum strain of 4530 με was registered in the SG 1.

In the B.6 beam the first visible crack was registered at a load of 69 kN. In Figures 16d and 16f are represented the $F-\varepsilon_s$ and $F-\varepsilon_f$ for beam B.6. The maximum strain in the stirrups was recorded in the SG 1, which was equal to 29090με, while in the ETS bars at 45-degrees, the maximum strain was recorded in the SG 1 and was equal to 4992 με.

Figure 17 shows that while A.5 beam has failed in bending with the yielding of the longitudinal reinforcement followed by the concrete crushing, in the B.5 beam, just after the yield initiation of the longitudinal reinforcement, the beam has failed by the formation of a shear failure crack. Like in the A.5 beam, in the B.5 beam the second stirrup from the support of the beam has ruptured. The crack pattern of B.6 was quite similar to the one of A.6, and both beams have failed in bending.

3. Prediction of experimental results

3.1 Shear resistance of RC beams according to ACI 440 and 318

To evaluate the nominal shear resistance of the tested beams (V_n), the recommendations of the ACI 440 (2008) were adopted by assuming that ETS bars can be regarded, from the strengthening point-of-view, like a fibre reinforced polymer (FRP) system. Therefore,

$$\phi V_n = \phi(V_c + V_s + \psi_f V_f) \tag{1}$$

where V_c, V_s and V_f are the contributions from the concrete, steel stirrups and ETS bars, respectively, ψ_f is a reduction factor applied to the contribution of the shear strengthening system, and ϕ is the strength-reduction factor required by ACI 318 (2008) that, for shear strengthening of concrete elements, assumes a value of 0.85. Since ETS bars have, in general, exceeded its yield strain and did not debond, a ψ_f value of 0.95, typical of FRP systems applied in order to guarantee full wrapped conditions for the section, is assumed in the present work (ACI 440, 2008). In equation (1), V_c has been computed using the upper limit indicated in Section 11.2.2.1 of the ACI 318 (2008), given by $V_c = 3.5\sqrt{f_c'} \cdot b_w \cdot d$, where f_c' is the concrete compressive strength, b_w is the web width, and d is the distance from the extreme compression fibre of the cross section to the centroid of the longitudinal reinforcement.

The contribution of the vertical steel stirrups was computed according to Section 11.4.7.2 of the ACI 318 Code, by applying the equation

$$V_s = \frac{A_v \cdot f_{yt} \cdot d}{s} \tag{2}$$

where A_v is the cross sectional area of steel stirrups of spacing s, and f_{yt} is the yield stress of the steel stirrup. When inclined bars are used as shear reinforcement,

$$V_s = \frac{A_v \cdot f_{yt} \cdot (\sin\alpha + \cos\alpha) \cdot d}{s} \tag{3}$$

where α is the angle between inclined stirrups and longitudinal axis of the member, and s is measured in direction parallel to longitudinal reinforcement. The contribution of ETS bars is evaluated by introducing convenient adjustments in equations (2) and (3):

$$V_f = \frac{A_f \cdot f_{yt} \cdot d}{s_f} \tag{4}$$

and

$$V_f = \frac{A_f \cdot f_{yt} \cdot (\sin\alpha + \cos\alpha) \cdot d}{s_f} \tag{5}$$

where A_f is the cross sectional area of the ETS bars of spacing s_f and f_{yt} is the yield stress of the ETS bar.

3.2 Shear resistance of RC beams according to the Eurocode 2 (2004)

In the case of the reference beams, the design value for the shear resistance, $V_{Rd,c}$, for members do not requiring shear reinforcement is determined from:

$$V_{Rd,c} = [C_{Rd,c}k(100\rho_l f_{ck} + k_1\sigma_{cp})^{1/3}]b_w d \geq (\mathrm{V}_{\min} + k_1\sigma_{cp})\, b_w d \tag{6}$$

where f_{ck} is the characteristic value of concrete compressive strength, $k = 1+\sqrt{200/d} \leq 2.0$ (width d in mm), $\rho_l = A_{sl}/b_w d \leq 0.02$, being A_{sl} the cross sectional area of the tensile reinforcement. The recommended value for $C_{Rd,c}$ is $0.18/\gamma_c$, where γ_c is the partial safety factor for concrete. Additionally, σ_{cp} is the stress due to the axial load, $k_1 = 0.15$ (recommended value) and $V_{\min} = 0.035k^{3/2} f_{ck}{}^{1/2}$.

The shear resistance of a member with shear reinforcement is obtained from:

$$V_{Rd} = V_{Rd,s} + V_{cdd} + V_{td} \tag{7}$$

where $V_{Rd,s}$ is the design value of the shear force that is sustained by the steel stirrups, V_{cdd} and V_{td} are the design values of the shear components of the force in the compression area and in the tensile reinforcement, respectively, in the case of an inclined compression chord. In the present work, rectangular cross-sections with no inclined chords were considered, since the depth of the cross section of the beams is constant. For reinforced concrete members with vertical steel stirrups, the $V_{Rd,s}$ is the smaller value between

$$V_{Rd,s} = \frac{A_{sw}}{s} \cdot z \cdot f_{ywd} \cdot \cot\theta \tag{8}$$

and

$$V_{Rd,\max} = \alpha_{cw} b_w z v_1 f_{cd} / (\cot\theta + \tan\theta) \tag{9}$$

For members with inclined shear reinforcement, the $V_{Rd,s}$ is the smaller value between

$$V_{Rd,s} = \frac{A_{sw}}{s} \cdot z \cdot f_{ywd} \cdot (\cot\theta + \cot\alpha)\sin\alpha \tag{10}$$

and

$$V_{Rd,\max} = \alpha_{cw} b_w z v_1 f_{cd} (\cot\theta + \tan\alpha) / (1 + \cot^2\theta) \tag{11}$$

where $V_{Rd,\max}$ is the design value of the maximum shear force that can be sustained by the member, limited by crushing of the compression struts; A_{sw} is the cross-sectional area of the shear reinforcement; s is the spacing of the stirrups; z is the lever arm (that may be considered as $z = 0.9 \cdot d$), f_{ywd} is the design value of the yield stress of the shear reinforcement; θ is the angle of the inclined struts ($1 \le \cot\theta \le 2.5$), α is the angle between the inclined bars and the axis of the beam; v_1 is a strength reduction factor to take into account that concrete is cracked in the shear region (considered as 0.6 for $f_{ck} < 60$ MPa); α_{cw} is a coefficient to take into account the stress state in the compression chord (recommended values of 1 for non-prestressed structures) and f_{cd} is the design value of concrete compressive strength.

To take into account the contribution of the ETS bars ($V_{Rd,f}$) for the shear strengthening of a shear reinforced element, in Equation (7) the term $V_{Rd,f}$ was also added:

$$V_{Rd,f} = \frac{A_{sf}}{s_f} \cdot z \cdot f_{ywd} \cdot (\cot\theta + \cot\alpha)\sin\alpha \tag{12}$$

where $V_{Rd,f}$ is the design value of the maximum shear force that can be sustained by the ETS bars, A_{sf} and f_{ywd} is the cross-sectional area and the design value of the yield stress of a ETS bar, and s_f is the spacing of ETS bars.

The shear resistance of the beams tested in the experimental program ($V^{\exp}$) is compared to the nominal shear resistance (V_n) given by ACI 318 (2008) and Eurocode 2 (2004) formulations, and the results are compared in Table 5. Since the contribution of the stirrups and ETS bars depends on the inclination of the shear failure crack, the two extreme limits are considered: $\cot\theta = 2.5 \Rightarrow \theta = 21.8^\circ$ and $\cot\theta = 1.0 \Rightarrow \theta = 45^\circ$. According to the formulations of the ACI 318 (2008) and ACI 440 (2008), most of the values of $V^{\exp}/V_n$ were higher than one (safety condition) and an average value of about 1.22 for $V^{\exp}/V_n$ was obtained. The unique unsafe value $\left(V^{\exp}/V_n = 0.97\right)$ was obtained in B.3 beam.

Following the recommendations of Eurocode 2 (2004) design values should be adopted for the strength properties of the intervening materials, and for the safety factors γ_c and γ_s the values of 1.5 and 1.15 are proposed. Taking into account these suggestions, the application of the Eurocode 2 formulation has conducted to 1.63 and 3.34 for $V^{\exp}/V_{Rd}$, respectively, for $\theta = 21.8^\circ$ and $\theta = 45^\circ$. Therefore, it can be concluded that, in general, ACI and Eurocode have predicted a shear resistance lower than the one registered experimentally, but ACI has conducted to more uniform values of $V^{\exp}/V_n$ than Eurocode 2 in terms of $V^{\exp}/V_{Rd}$.

4. Comparison between ETS, NSM and EBR techniques for the shear strengthening of RC beams

Recently Dias and Barros (2012) assessed the effectiveness of EBR and NSM techniques for the shear strengthening of RC beams. For this purpose, 9 T cross section beams reinforced according to the NSM technique, with a ρ_{fw} that varied from 0.07 to 0.16%, and 3 T cross section beams reinforced according to the EBR technique, with a ρ_{fw} that changed from 0.07 to 0.21% were tested. Fig. 18 represents the relationship between the strengthening efficacy, $\Delta F_{max}/F_{max}^{2S\text{-}R}$ (where $\Delta F_{max}/F_{max}^{2S\text{-}R}$ is the load carrying capacity of the reference beam) provided by the CFRP arrangements, and the ρ_{fw} for the analyzed NSM and EBR shear strengthening configurations. This figure shows that, regardless the ρ_{fw}, the arrangement of laminates at 45º was the most effective among the adopted CFRP shear strengthening configurations, and the EBR was not so effective as NSM technique. It is also observed that inclined laminates were more effective than vertical laminates. This is justified by the orientation of the shear failure cracks that had a tendency to be almost orthogonal to the inclined laminates. Furthermore, for vertical laminates the total resisting bond length of the CFRP is lower than for inclined laminates. The NSM beams with the lowest percentage of inclined laminates had better performance than the EBR beam with the highest percentage of CFRP. Fig. 10 also shows that, independently of the orientation of the laminates, and for the range of ρ_{fw} values considered in the present experimental program, $\Delta F_{max}/F_{max}^{2S\text{-}R}$ has increased, almost linearly, with the increase of ρ_{fw}. This tendency was verified in both NSM and EBR shear strengthening techniques.

Taking into account that the average value of the strengthening efficacy of the ETS technique was 54%, these results indicate that ETS technique was a more effective than the EBR and NSM. For a more reliable comparison of the strengthening efficacy of the ETS, NSM and EBR techniques, series of T cross section beams shear strengthened according to the ETS technique are being prepared, and the results will be compared with those collected in a data base (http://dabasum.civil.uminho.pt/).

When comparing the strengthening efficacy of these shear strengthening techniques it is also important to verify that ETS bars are more protected against the aggressiveness of external agents, like fire, vandalism acts and environmental conditions, than the strengthening elements of NSM and EBR. The direct and long term (maintenance) costs should be also considered in this comparison.

5. Conclusions

This study presents the relevant results of an experimental program for the assessment of the effectiveness of the Embedded Through-Section (ETS) technique for the shear strengthening of reinforced concrete beams. The influence of the following parameters was investigated: spacing of the existing steel stirrups (225 and 300 mm); spacing (225 and 300 mm) and inclination of the strengthening bars (vertical and 45-degree); width of the cross section of the beam. When available experimental data on the use of EBR and NSM technique for the shear resistance of RC beams is considered, the obtained results show that, for the same shear strengthening ratio, ETS technique provides increase levels of load carrying and deflection capacities higher than those FRP-based shear strengthening techniques. This technique can be used to avoid the occurrence of shear failure in RC beams, by converting this brittle failure mode in a ductile bending failure mode. Furthermore, in the ETS technique it can be used low cost steel bars bonded to concrete with cement based matrix that incorporates a small percentage of resin based-component. Since ETS steel bars have a relatively thick concrete cover, corrosion and injuries due to vandalism acts are not a concern, and higher protection to fire is assured.

The capability of the ACI and Eurocode 2 design guidelines to evaluate the shear resistance of the tested beams was appraised by using the experimental results. A good agreement between the experimental and analytical values was obtained, mainly when using the ACI 318 approach.

6. Acknowledgements

The study reported in this paper is part of the research project “DURCOST”, PTDC/ECM/105700/2008, supported by FCT. The authors wish to acknowledge the support provided by the “Empreiteiros Casais”, Secil (Unibetão, Braga), and Sika PortugalCompanies. The first author would like to acknowledge the National Council for Scientific and Technological Development (CNPq) – Brazil for financial support for scholarship (GDE 200953/2007-9).

References

ACI Committee 318 (2008). “Building code requirements for structural concrete and Commentary (ACI 318-08)”, Reported by committee 318, American Concrete Institute, Detroit.

ACI Committee 440 (2008). “Guide for the design and construction of externally bonded FRP systems for strengthening concrete structures”. American Concrete Institute; 2008. 80 p.

ASTM 370 (2002). “Standard test methods and definitions for mechanical testing of steel products”, American Society for Testing and Materials.

Barros, J.A.O., Dalfré, G.M., Trombini, E., Aprile, A. (2008). “Exploring the possibilities of a new technique for the shear strengthening of RC elements”. *Proceedings of the International Conference Challenges for Civil Construction*, University of Porto, Portugal.

Barros, J.A.O.; Dias, S.J.E.; Lima, J.L.T. (2007). “Efficacy of CFRP-based techniques for the flexural and shear strengthening of concrete beams.” Cement and Concrete Composites Journal, 29(3), 203-217.

Barros, J.A.O.; Dias, S.J.E. (2006). “Near surface mounted CFRP laminates for shear strengthening of concrete beams.” Cement and Concrete Composites Journal, 28(3), 276-292.

Bianco, V., Barros, J.A.O., Monti, G. (2009). “Bond model of NSM-CFRP in the context of the shear strengthening of RC beams.” ASCE Structural Engineering Journal, 135(6), 619-631.

Chaallal, O., Mofidi, A., Benmokrane, B., Neale, K. (2011). “Embedded Through-Section FRP Rod Method for Shear Strengthening of RC Beams: Performance and Comparison with Existing Techniques.” *Journal of Composutes for Construction*, May/June, 374-383.

Dias, S.J.E.; Barros, J.A.O. (2012). “Experimental behaviour of RC beams shear strengthened with NSM CFRP laminates.” Strain - An International Journal for Experimental Mechanics, 48(1), 88-100.

Eurocode 2: Design of concrete structures - part 1: General rules and rules for buildings EN 1992-1-1:2004:E. Brussels: European Committee for Standardization, December (2004).

ISO 527-2 (1993). “Plastics - Determination of Tensile Properties - Part 2: Test Conditions for Moulding and Extrusion Plastics.” International Organization for Standardization (ISO), Geneva, Switzerland.

LNEC NP-E397 (1993). Concrete - Assessment of the elasticity modulus under uniaxial compression. Laboratório Nacional de Engenharia Civil, in Portuguese.

Dalfré, G.M.; Barros, J.A.O.; Machado, D. (2011). “Steel bar – concrete bond behavior in the context of the ETS shear strengthening technique for RC beams.” 53º Brazilan Conference on Concrete – IBRACON 2011..

Trombini, E. (2008). “Indirect assessment of the performance of a shear strengthening technique for RC structures.” MSc thesis, Università degli Studi di Ferrara, Italy.

Valerio, P., Ibell, T.J., Darby, A.P. (2005). “Shear Assessment and Strengthening of Contiguous-Beam Concrete Bridges Using FRP Bars”. *Proceedings of the FRPRCS-7*, 7th International Symposium on Fiber Reinforced Polymer Reinforcement for Reinforced Concrete Structures, Kansas City, EUA, 825 – 848.

Valerio, P., Ibell, T. J., Darby, A. P. (2009). “Deep embedment of FRP for concrete shear strengthening”. *Proceedings of the Institution of Civil Engineers Structures and Buildings*, 162, SB5, 311–321.

NOTATION

Roman upper case letters

A_{sl}	cross sectional area of the longitudinal steel bars
b_w	web width
d	distance from the extreme compression fibre of the cross section to the centroid of the longitudinal reinforcement
A_{sw}	cross sectional area of the two arms of a steel stirrup
s_w	spacing between stirrups
A_f	cross sectional area of a ETS shear strengthening bar
s_f	spacing between ETS bars
a	shear span
F	applied load
f_{cm}	average compressive strength
$F_{\max}$	maximum value of the load registered in the load cell during the experimental program
$F_{\max}^{REF}$	maximum load supported by the reference beam
V_n	nominal shear resistance of the tested beams
V_c	shear resistance attributable to the concrete
V_s	shear resistance attributable to the steel stirrups
V_f	shear resistance attributable to the ETS bars
A_v	cross sectional area of steel stirrups by ACI 318
s	spacing between stirrups by ACI 318
f_{yt}	yield stress of the steel stirrup by ACI 318
A_f	cross sectional area of the ETS bars by ACI 440
s_f	spacing between stirrups by ACI 440

$V_{Rd,c}$ shear resistance for members not requiring shear reinforcement by EC2

f_{ck} characterist value of concrete compressive strength

$V_{Rd,s}$ design value of the shear force that is sustained by the steel stirrups

V_{cdd} design values of the shear components of the force in the compression area

V_{td} design values of the shear components of the force in the tensile reinforcement

$V_{Rd,\max}$ design value of the maximum shear force that can be sustained by the member

z lever arm

f_{ywd} design value of the yield stress of the shear reinforcement

f_{cd} the design value of concrete compressive strength

$V_{Rd,f}$ design value of the maximum shear force that can be sustained by the ETS bars

A_{sf} cross-sectional area of a ETS bar

f_{ywd} design value of the yield stress of a ETS bar

$V^{\exp}$ shear resistance of the beams tested in the experimental program

$V^{\exp}/V_n$ ratio between the shear resistance of the beams tested in the experimental program and analytical shear resistance obtained by the ACI and Eurocode 2 recommendations.

Greek lower case letters

ρ_{sl} longitudinal steel reinforcement ratio

ρ_{sw} shear reinforcement ratio

ρ_{fw} ETS strengthening ratio

θ_f inclination of the strengthening bars with respect to the longitudinal axis of the beam

$\delta_{F\max}$ deflection of the loaded section at $F_{\max}$

$\delta_{F\max}^{REF}$ deflection of the loaded section of the reference beam at $F_{\max}$

$\varepsilon_{s,F\max}$ maximum strains in the steel stirrups at $F_{\max}$

$\varepsilon_{f,F\max}$ maximum strains in the ETS bars at $F_{\max}$

$\varepsilon_{s,\max}$ maximum strains in the stirrups up to the failure of the beams

$\varepsilon_{f,\max}$ maximum strains in the ETS bars up to the failure of the beams

ψ_f reduction applied to the contribution of the shear strengthening system

ϕ strength-reduction factor required by ACI 318

α angle between inclined stirrups and longitudinal axis of the beam

γ_c partial safety factor for concrete

γ_s partial safety factor for steel

θ angle of the inclined struts

α angle between the inclined bars and the axis of the beam

α_{cw} coefficient to take into account the stress state in the compression chord

ν_1 strength reduction factor to take into account that concrete is cracked in the shear region

σ_{cp} stress due to the axial load

Greek upper case letters

$\Delta F_{\max} / F_{\max}^{REF}$ ratio between the increase in terms of load carrying capacity provided by the shear reinforcing system

$\Delta F_{\max}$ maximum load supported by the strengthened beam

$\Delta\delta_{F\max} / \delta_{F\max}^{REF}$ ratio between the increase in terms of deflection capacity provided by the shear reinforcing system

$\Delta\delta_{F\max}$ deflection of the the loaded section of the strengthened beam at $F_{\max}$

List of Tables

Table 1 - General information of the beams

Beams ID	150 x 300 mm^2					300 x 300 mm^2				
	Age of the strengthening when the beam was tested (days)	ρ_{sl} (%)	ρ_{sw} (%)	ρ_{fw} (%)	Batch	Age of the s trengthening when the beam was tested (days)	ρ_{sl} (%)	ρ_{sw} (%)	ρ_{fw} (%)	Batch
Reference	------	2.50	0.00	0.00	1	------	1.88	0.00	0.00	1
S300.90	------	2.50	0.13	0.00	1	------	1.88	0.06	0.00	1
E300.90	34	2.50	0.00	0.17	1	65	1.88	0.00	0.11	1
E300.45	34	2.50	0.00	0.25	2	64	1.88	0.00	0.16	2
S300.90/ E300.90	33	2.50	0.13	0.17	1	69	1.88	0.06	0.11	1
S300.90/ E300.45	29	2.50	0.13	0.25	2	68	1.88	0.06	0.16	2
S225.90	------	2.50	0.17	0.00	2					
S225.90/ E225.90	35	2.50	0.17	0.23	2					

Table 2 – Materials properties

Steel Reinforcement						Concrete	
Steel bar diameter (∅s)	Modulus of elasticity (GPa)	Yield stress (MPa)	Strain at yield stress (‰)	Tensile strength (MPa)	Bars ID	Batch ID	f_{cm} (MPa)
12 mm	206.62 (1.84)	484.68 (1.26)	2.35 (3.21)	655.53 (0.91)	Longitudinal reinforcement	1	30.78 (4.90)
25 mm	216.19 (9.83)	507.68 (0.96)	2.27 (4.76)	743.41 (1.31)	Longitudinal reinforcement	2	28.81 (4.55)
6 mm	206.07 (6.72)	559.14 (1.00)	2.75 (6.54)	708.93 (1.44)	Stirrups	Adhesive	
8 mm	212.36 (4.29)	566.50 (4.17)	2.66 (6.97)	675.73 (2.03)	ETS strengthening bar	Modulus of elasticity (GPa)	3.94 (9.82)
10 mm	205.16 (3.25)	541.60 (0.91)	2.66 (3.98)	643.23 (0.39)	ETS strengthening bar	Tensile strength (MPa)	26.29 (10.62)

(value) Coefficient of Variation (COV) = (Standard deviation/Average) x 100; f_{cm} = mean cylinder concrete compressive strength

Table 3 – Experimental results

Series		Specimen	$F_{\max}$ (kN)	$\frac{\Delta F_{\max}}{F_{\max}^{REF}}$ (%)	$\delta,_{F\max}$ (mm)	$\frac{\Delta\delta_{F\max}}{\delta_{F\max}^{REF}}$ (%)	V_n (kN)	V_c (kN)	V_s (kN)	V_f (kN)	$\varepsilon_{s,F\max}$ (‰)	$\varepsilon_{f,F\max}$ (‰)	$\varepsilon_{s,\max}$ (‰)	$\varepsilon_{f,\max}$ (‰)
Series A	A.1	Reference	108.86	------	4.01	------	65.32	65.32	--------	--------	------	------	--------	--------
	A.2	S300.90	164.67	51.27	8.40	109.58	98.80		33.48	--------	2.73 (S2)	--------	2.95 (S2)	--------
	A.3	E300.90	160.78	47.69	6.97	73.96	96.47		--------	31.15	--------	2.15 (1)	--------	8.38 (3)
	A.4	E300.45	203.98	87.38	12.04	200.25	122.39		--------	57.07	--------	2.07 (4)	--------	4.12 (4)
	A.5	S300.90/ E300.90	231.83	112.96	13.12	227.18	139.10		33.48	40.30	2.44 (S2)	2.57 (1)	3.08 (S2)	2.68 (1)
	A.6	S300.90/ E300.45	244.41	124.52	14.00	249.21	146.65		33.48	47.85	2.41 (S1)	15.64 (4)	2.70 (S1)	17.29 (4)
	A.7	S225.90	180.31	65.63	9.92	147.32	108.19		42.87	--------	4.27 (S2)	--------	4.56 (S2)	--------
	A.8	S225.90/ E225.90	244.17	124.30	14.44	260.10	146.50		42.87	38.31	2.08 (S3)	2.60 (1)	2.31 (S2)	4.70 (5)
Series B	B.1	Reference	203.36	------	4.45	------	122.02	122.02	--------	--------	------	------	--------	--------
	B.2	S300.90	232.31	14.24	5.56	24.94	139.39		17.37	--------	1.66 (S2)	--------	18.70 (S2)	--------
	B.3	E300.90	238.88	17.47	6.06	36.18	143.33		--------	21.31	--------	0.53 (1)	--------	1.13 (4)
	B.4	E300.45	336.19	65.32	9.42	111.68	201.71		--------	79.69	--------	1.97 (4)	--------	3.20 (4)
	B.5	S300.90/ E300.90	390.11	91.83	15.01	237.30	234.07		17.37	94.68	2.91 (S1)	2.54 (3)	3.27 (S2)	4.53 (1)
	B.6	S300.90/ E300.45	396.51	94.97	20.18	353.48	237.91		17.37	98.52	14.63 (S1)	4.77 (1)	29.09 (S1)	4.99 (1)

(value) = SG that registered the maximum strain at F_{max}.

Table 4 – Analytical *vs* experimental results for ETS technique.

Specimen			Experimental				Analytical									
							ACI					Eurocode 2				
			V_c (kN)	V_s (kN)	V_f (kN)	$V^{\exp}$ (kN)	V_c (kN)	V_s (kN)	V_f (kN)	V_n (kN)	$\frac{V^{\exp}}{V_n}$	$V_{Rd,c}$ (kN)	$V_{Rd,s}$ (kN)	$V_{Rd,f}$ (kN)	V_{Rd} (kN)	$\frac{V^{\exp}}{V_{Rd}}$
Series A	A.1	Reference	65.32	--------	--------	65.32	53.77	--------	--------	53.77	1.21	31.51	--------	--------	31.51	2.07
	A.2	S300.90		33.48	--------	98.80	53.77	23.42	--------	77.19	1.28	0.00	(53.93) [21.58]	--------	(53.93) [21.58]	(1.83) [4.58]
	A.3	E300.90		--------	31.15	96.47	53.77	--------	29.93	83.70	1.15	0.00	--------	(72.55) [29.04]	(72.55) [29.04]	(1.33) [3.32]
	A.4	E300.45		--------	57.07	122.39	52.02	--------	42.32	94.34	1.30	0.00	--------	(71.82) [41.06]	(71.82) [41.06]	(1.70) [2.98]
	A.5	S300.90/ E300.90		33.48	40.30	139.10	53.77	23.42	29.93	107.12	1.30	0.00	(53.93) [21.58]	(72.55) [29.04]	(126.48) [50.62]	(1.10) [2.75]
	A.6	S300.90/ E300.45		33.48	47.85	146.65	52.02	23.42	42.32	117.76	1.25	0.00	(53.93) [21.58]	(71.82) [41.06]	(125.75) [62.64]	(1.17) [2.34]
	A.7	S225.90		42.87	--------	108.19	52.02	31.21	--------	83.23	1.30	0.00	(71.90) [28.78]	--------	(71.90) [28.78]	(1.50) [3.76]
	A.8	S225.90/ E225.90		42.87	38.31	146.50	52.02	31.21	39.89	123.12	1.19	0.00	(71.90) [28.78]	(96.73) [38.72]	(168.63) [67.50]	(0.87) [2.17]
Series B	B.1	Reference	122.02	--------	--------	122.02	107.45	--------	--------	107.45	1.14	61.70	--------	--------	61.70	1.98
	B.2	S300.90		17.37	--------	139.39	107.45	23.42	--------	130.87	1.07	0.00	(53.93) [21.58]	--------	(53.93) [21.58]	(2.58) [6.46]
	B.3	E300.90		--------	21.31	143.33	107.45	--------	40.07	147.52	0.97	0.00	--------	(97.13) [38.88]	(97.13) [38.88]	(1.48) [3.69]
	B.4	E300.45		--------	79.69	201.71	103.96	--------	56.66	160.62	1.26	0.00	--------	(96.15) [54.98]	(96.15) [54.98]	(2.10) [3.67]
	B.5	S300.90/ E300.90		17.37	94.68	234.07	107.45	23.42	40.07	170.94	1.37	0.00	(53.93) [21.58]	(97.13) [38.88]	(151.06) [60.46]	(1.55) [3.87]
	B.6	S300.90/ E300.45		17.37	98.52	237.91	103.96	23.42	56.66	184.04	1.29	0.00	(53.93) [21.58]	(96.15) [54.98]	(150.08) [76.56]	(1.58) [3.11]

() values determined with $\cot\theta = 2.5 \Rightarrow \theta = 21.8^\circ$; []values determined with $\cot\theta = 1.0 \Rightarrow \theta = 45^\circ$

LIST OF FIGURES

18 – Strengthening efficacy ($\Delta F_{max}/F_{max}^{2S\text{-}R}$) *vs* CFRP percentage (ρ_{fw}) (Dias and Barros 2012)

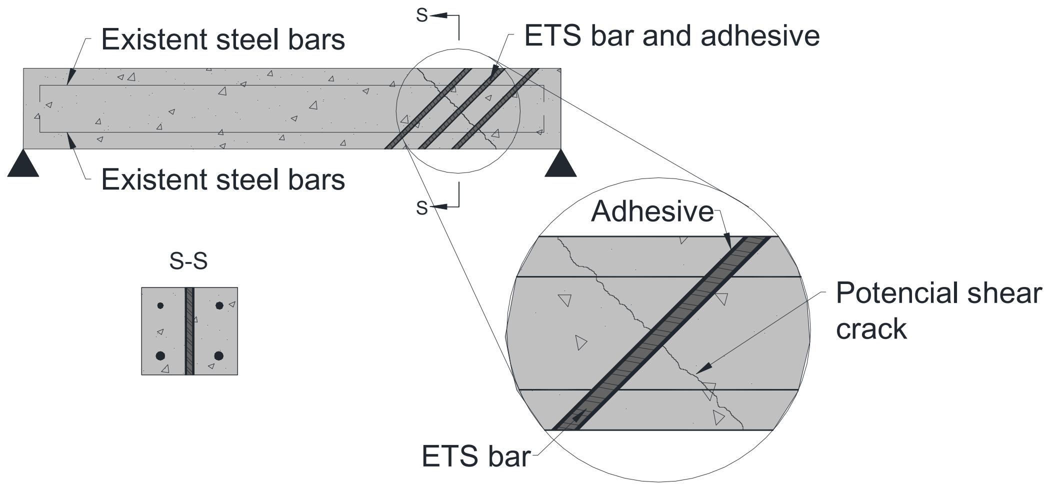

Figure1 - ETS strengthening technique concept for the shear strenghthening of RC beams.

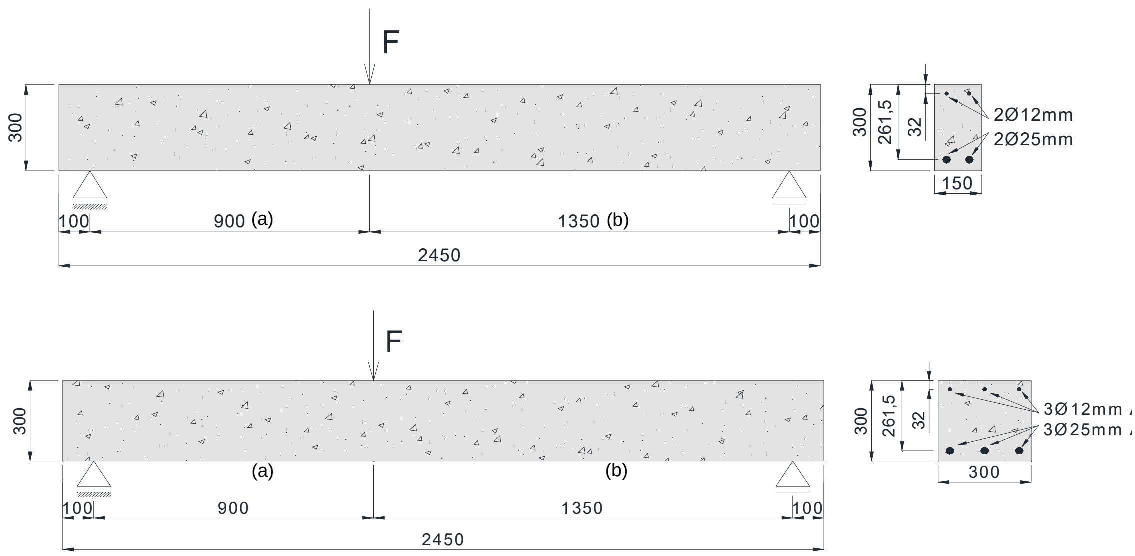

Figure 2 – Test configuration (all dimensions are in mm)

	Beam´s designation		Shear strengthening system	Shear strengthening arrangements	Shear span reinforcement/ strengthening
A Series Beams	A.1	Reference	-----------	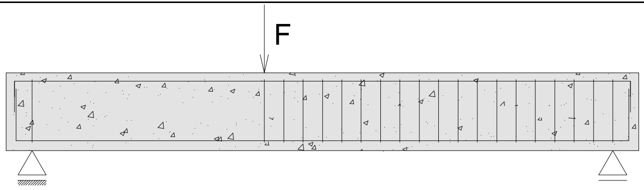	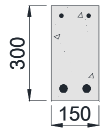
	A.2	S300.90	Stirrups at 90° (2ϕ6 mm, 2 arms, 300 mm spacing)	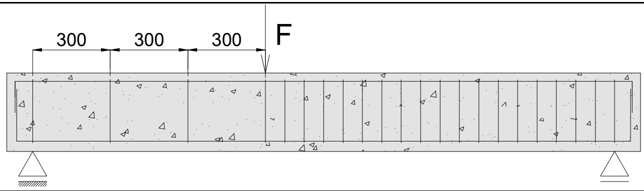	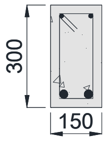
	A.3	E300.90	ETS strengthening bars at 90° (3ϕ10 mm, 300 mm spacing)	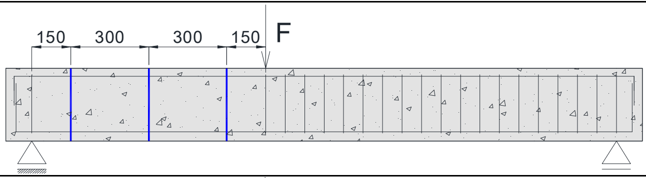	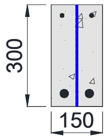
	A.4	E300.45	ETS strengthening bars at 45° (3ϕ10 mm, 300 mm spacing)	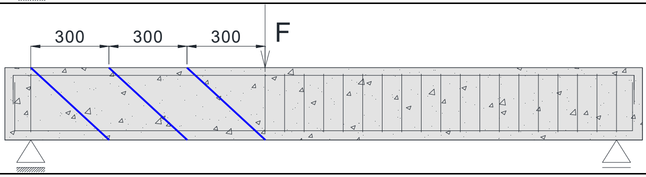	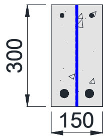
	A.5	S300.90/ E300.90	Stirrups at 90° (2ϕ6 mm, 2 arms, 300 mm spacing) ETS strengthening bars at 90° (3ϕ10 mm, 300 mm spacing)	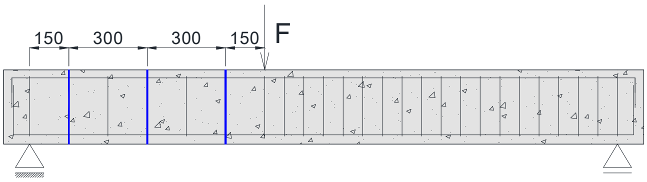	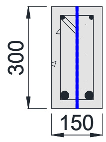
	A.6	S300.90/ E300.45	Stirrups at 90° (2ϕ6 mm, 2 arms, 300 mm spacing) ETS strengthening bars at 45° (3ϕ10 mm, 300 mm spacing)	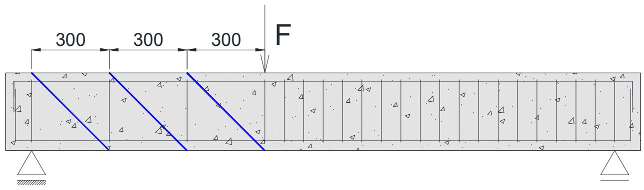	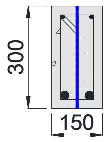
	A.7	S225.90	Stirrups at 90° (3ϕ6 mm, 2 arms, 225 mm spacing)	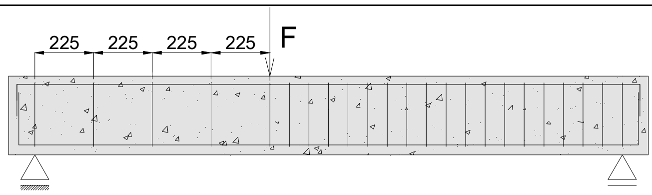	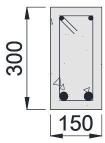
	A.8	S225.90/ E225.90	Stirrups at 90° (3ϕ6 mm, 2 arms, 225 mm spacing) ETS strengthening bars at 90° (4ϕ10 mm, 225 mm spacing)	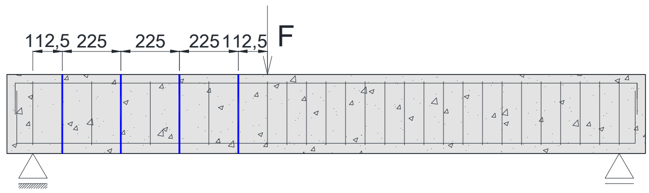	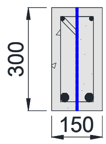

Figure 3 - General information about A series (all dimensions are in mm)

	Beam´s designation		Shear strengthening system	Shear strengthening arrangements	Shear span reinforcement/ strengthening
B Series	B.1	Reference	-----------	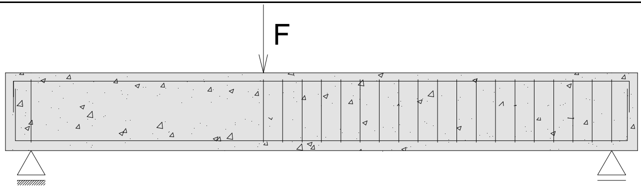	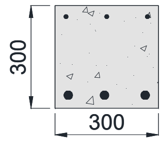
	B.2	S300.90	Stirrups at 90° (2ϕ6 mm, 2 arms, 300 mm spacing)	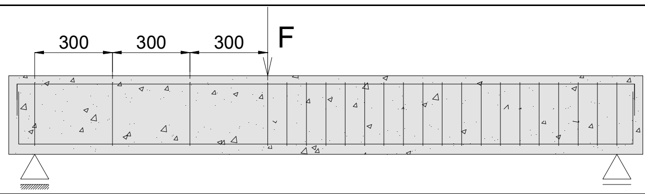	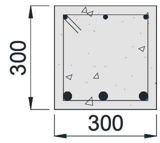
	B.3	E300.90	ETS strengthening bars at 90° (2 x 3ϕ8 mm, 300 mm spacing)	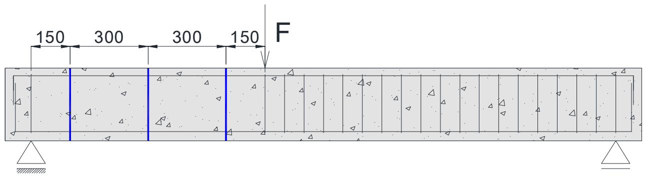	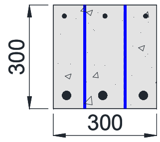
	B.4	E300.45	ETS strengthening bars at 45° (2 x 3ϕ8 mm, 300 mm spacing)	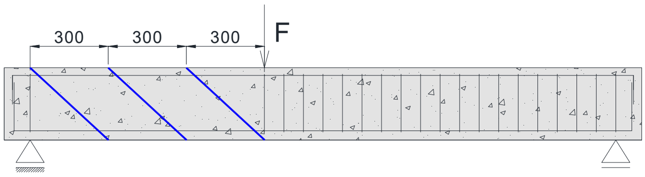	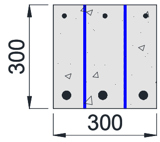
	B.5	S300.90/ E300.90	Stirrups at 90° (2ϕ6 mm, 2 arms, 300 mm spacing) ETS strengthening bars at 90° (2 x 3ϕ8 mm, 300 mm spacing)	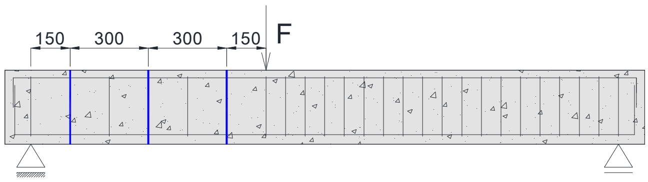	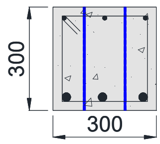
	B.6	S300.90/ E300.45	Stirrups at 90° (2ϕ6 mm, 2 arms, 300 mm spacing) ETS strengthening bars at 45° (2 x 3ϕ8 mm, 300 mm spacing)	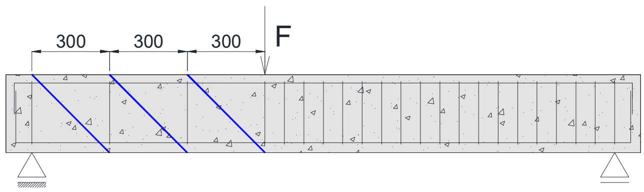	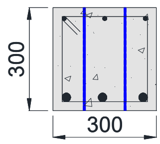

Figure 4 - General information about B series (all dimensions are in mm)

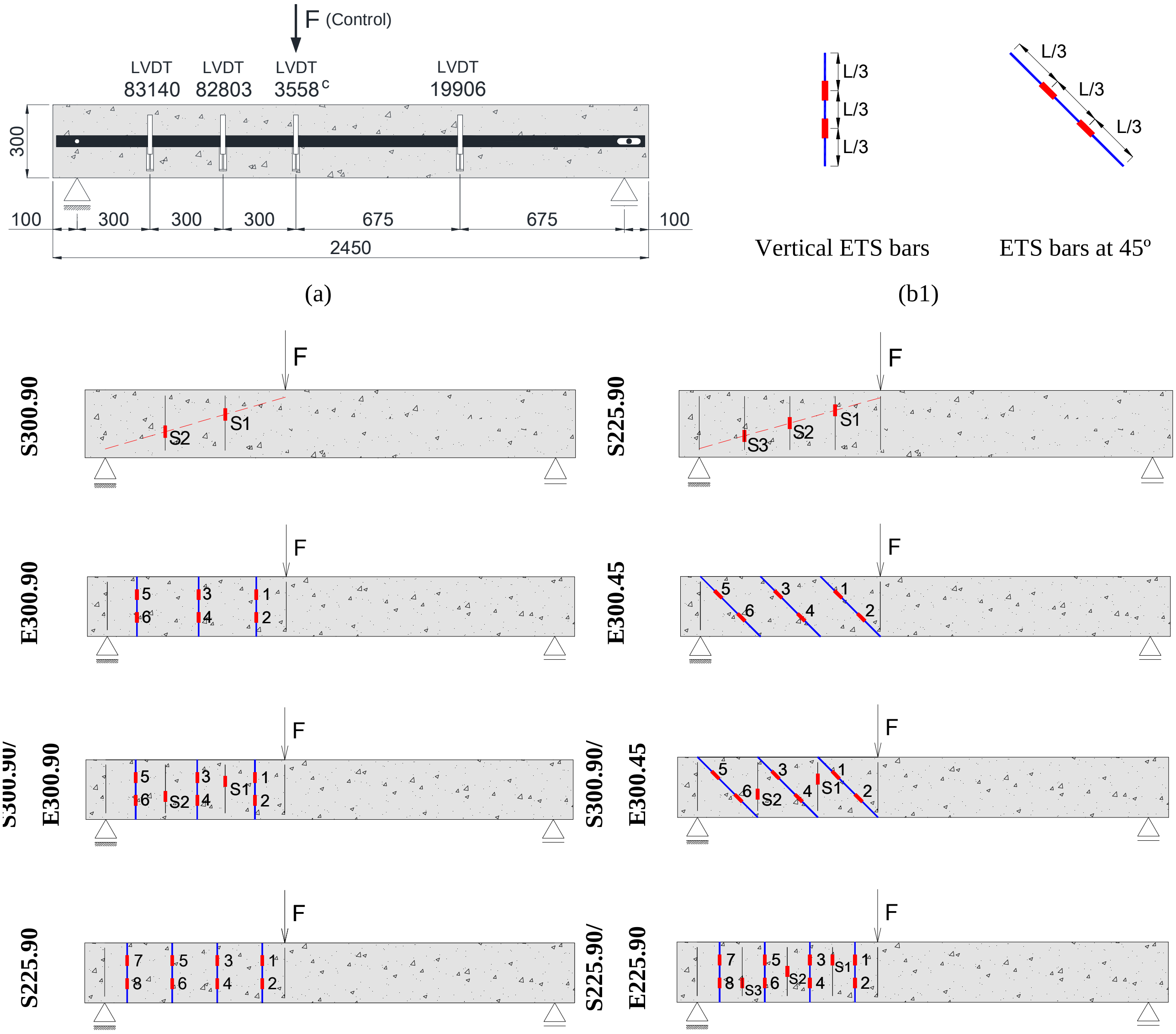

(b2)

Figure 5 - Monitoring system: (a) arrangement of the displacement transducers and (b1-b2) positions of the strain gauges in the monitored stirrups and ETS bars (all dimensions are in mm)

(a) (b) (c)

Figure 6 – ETS strengthening technique: (a) drilling the holes, (b) compressed air to clean the holes and (c) the hole is filled with adhesive and the ETS strengthening bar

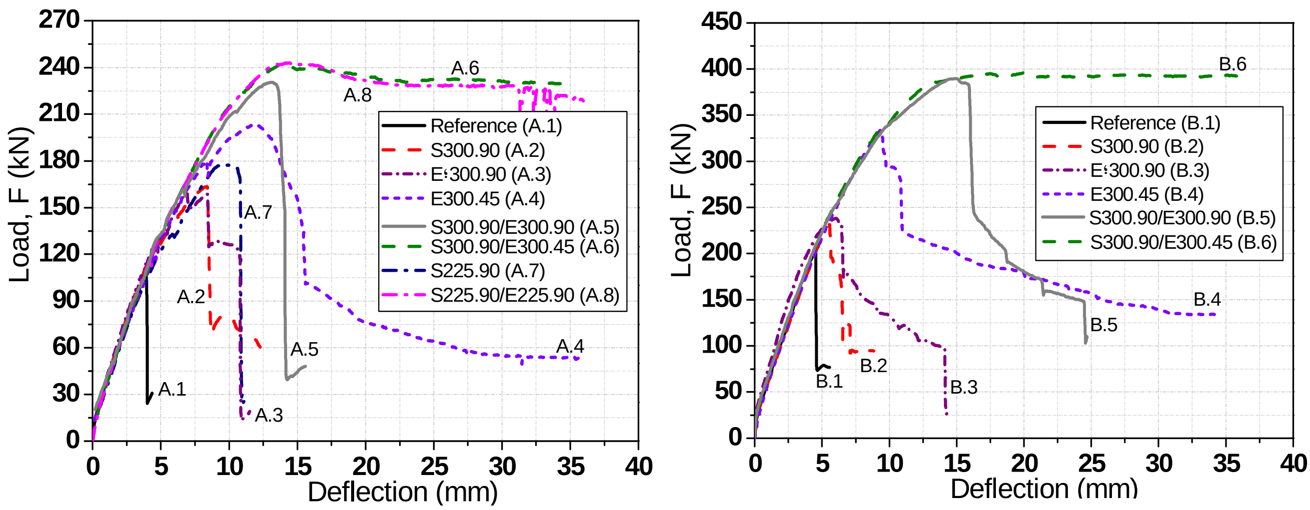

(a) (b)

Figure 7 – Relationship between the load and the loaded section deflection for series:

(a) A, and (b) B

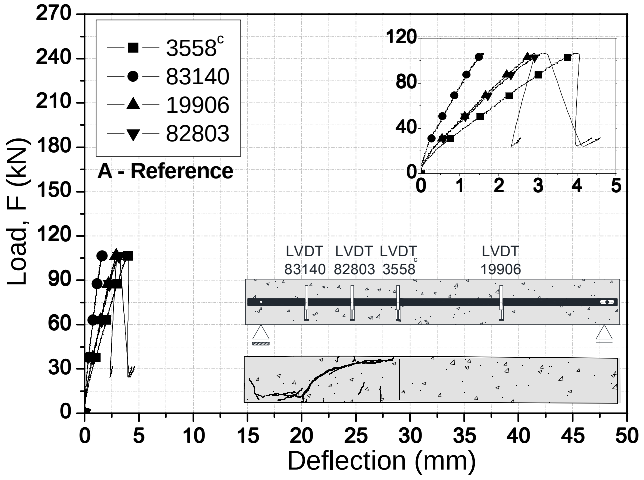

Figure 8 — Relationship between the applied load and the deflections of the Reference beam of series A

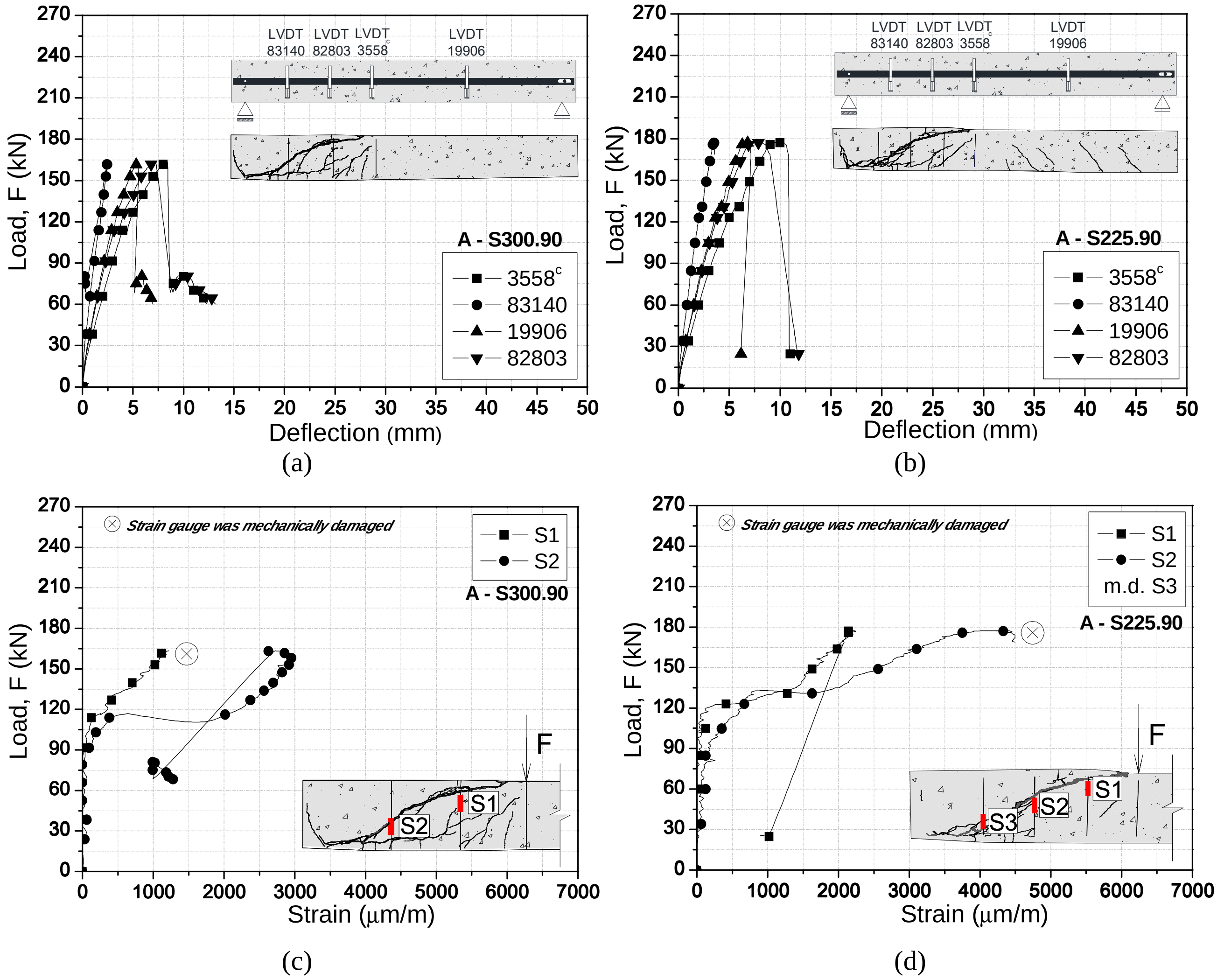

Figure 9 — Relationship between applied load and deflections (a-b), and relationship between applied load and tensile strains in the steel stirrups (c-d) for the specimens A.2 and A.7, respectively (m.d.=mechanically damaged)

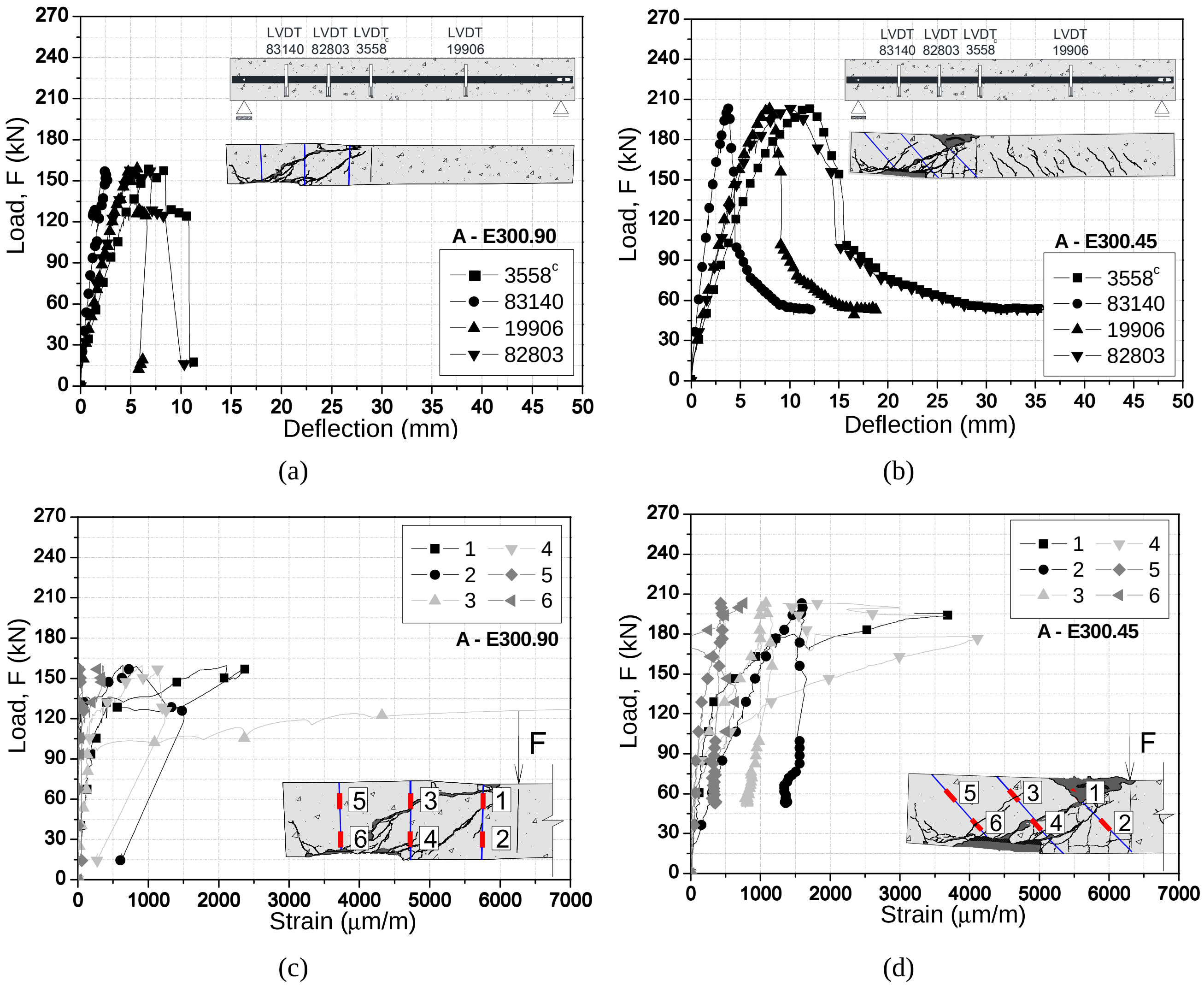

Figure 10 — Relationship between applied load and deflections (a-b), and relationship between applied load and tensile strains in the ETS strengthening bars (c-d) for the specimens A.3 and A.4, respectively

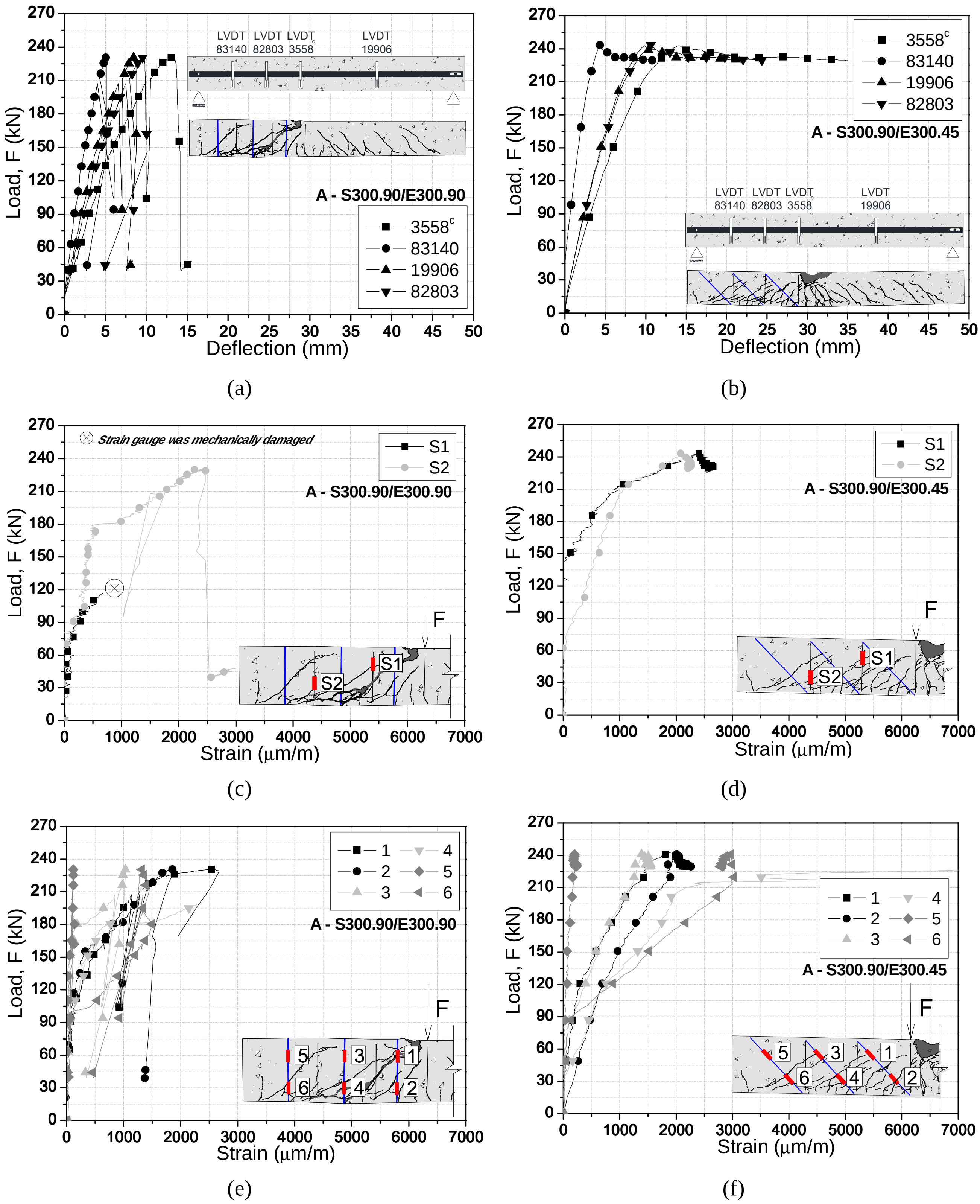

Figure 11 — Relationship between applied load and deflections (a-b), and relationship between applied load and tensile strains in the steel stirrups (c-d) and ETS strengthening bars (e-f) for the specimens A.5 and A.6, respectively

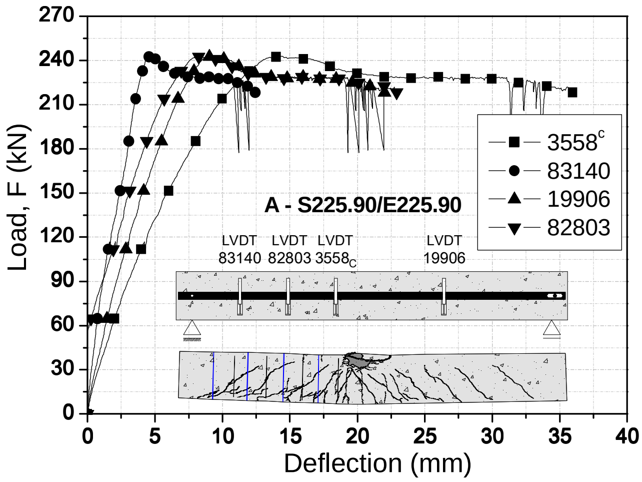

(a)

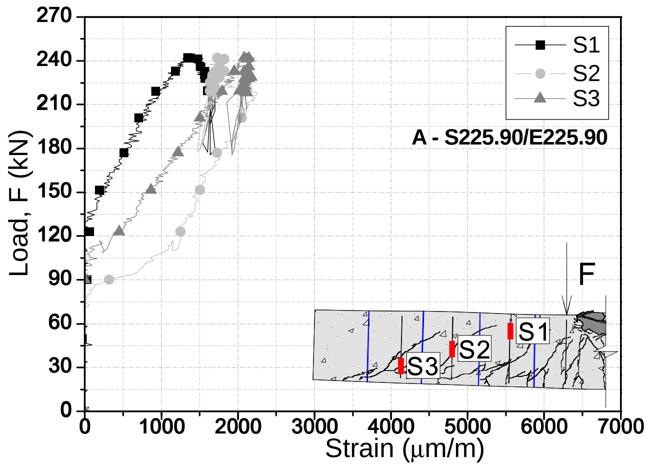

(b)

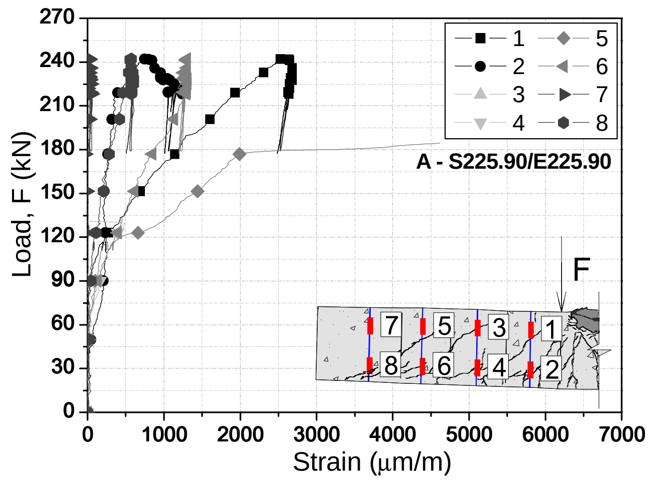

(c)

Figure 12 — Relationship between applied load and deflections (a), and relationship between applied load and tensile strains in the steel stirrups (b) and ETS strengthening bars (c) for the specimen A.8

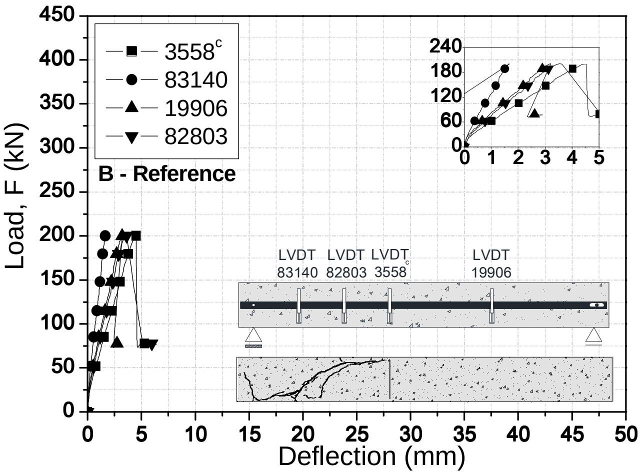

Figure 13 — Relationship between the applied load and the deflections of the Reference beam (B.1) of B series

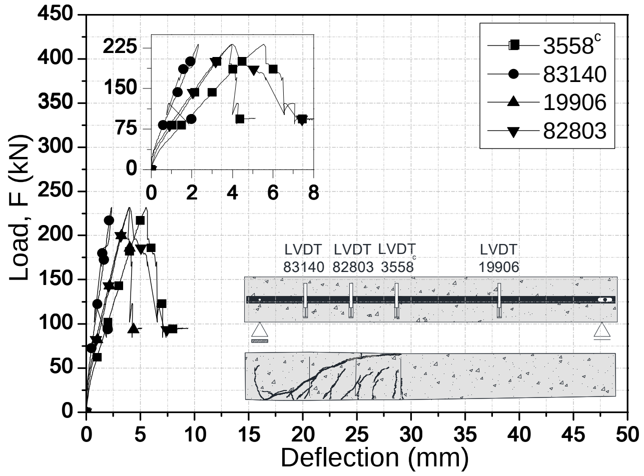

(a)

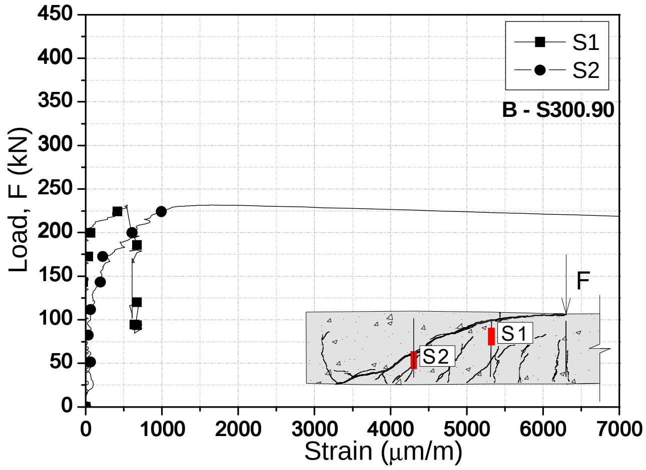

(b)

Figure 14 — Relationship between the applied load and the deflections (a), and relationship between the applied load and tensile strains in the steel stirrups (b) for the specimens B.2

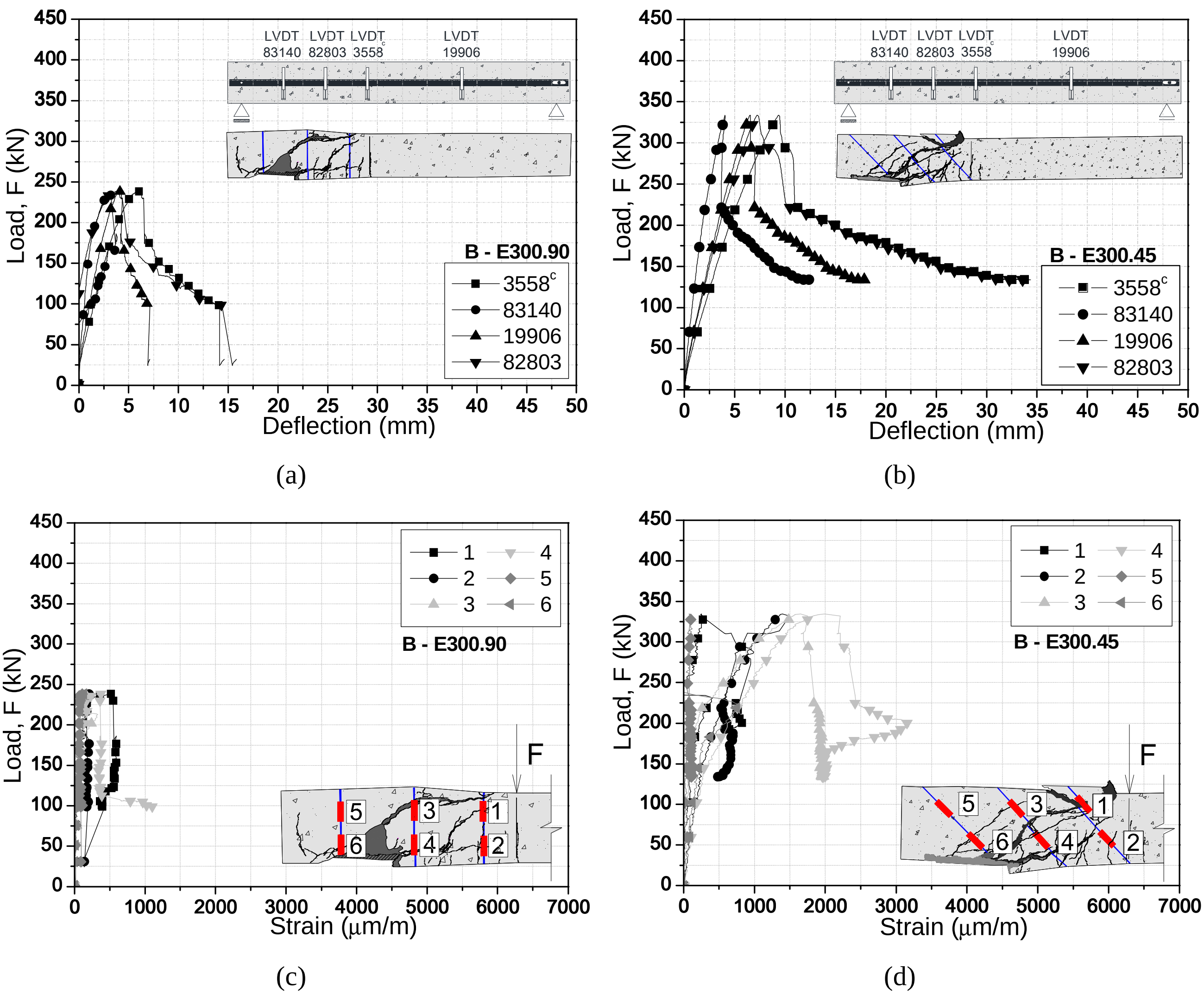

Figure 15 — Relationship between applied load and deflections (a-b), and relationship between applied load and tensile strains in the ETS strengthening bars (c-d) for the specimens B.3 and B.4, respectively

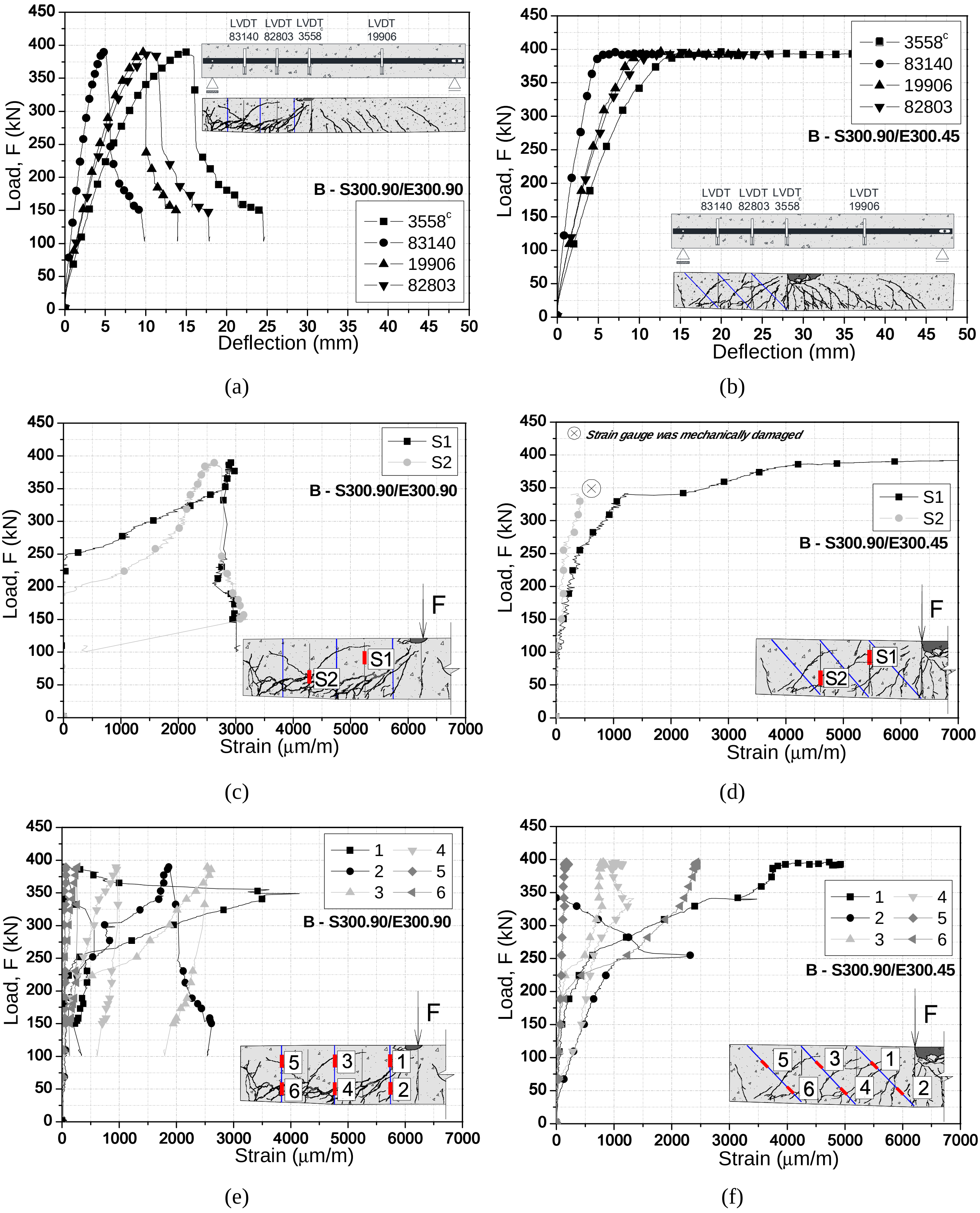

Figure 16 — Relationship between applied load and deflections (a-b), and relationship between applied load and tensile strains in the steel stirrups (c-d) and ETS strengthening bars (e-f) for the specimens B.5 and B.6, respectively

Beam´s ID	150 x 300 mm^2 (A Series)	300 x 300 mm^2 (B Series)
Reference (A.1, B.1)	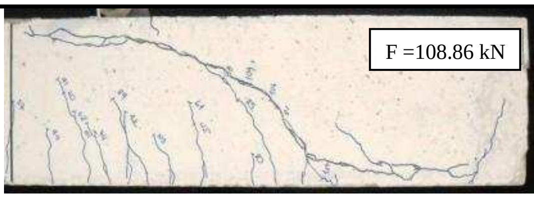	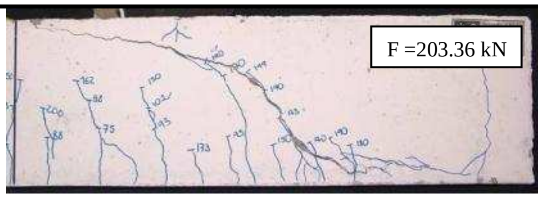
S300.90 (A.2, B.2)	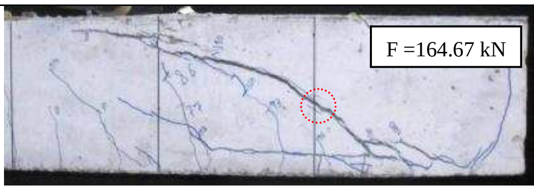	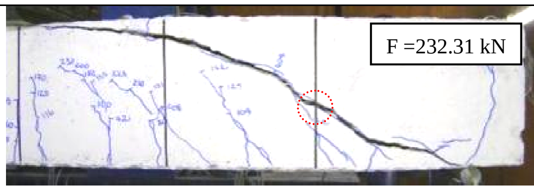
E300.90 (A.3, B.3)	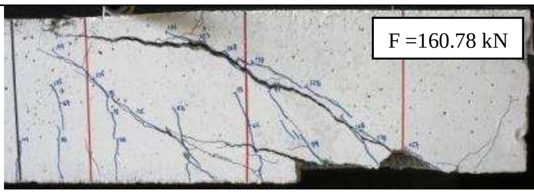	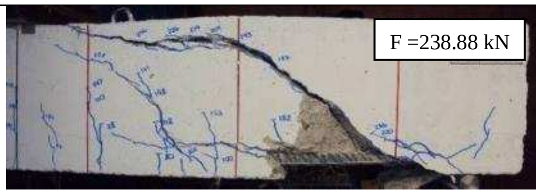
E300.45 (A.4, B.4)	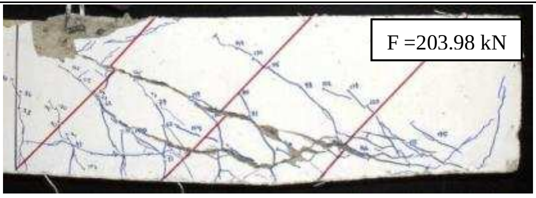	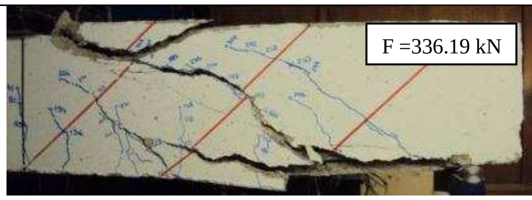
S300.90/ E300.90 (A.5, B.5)		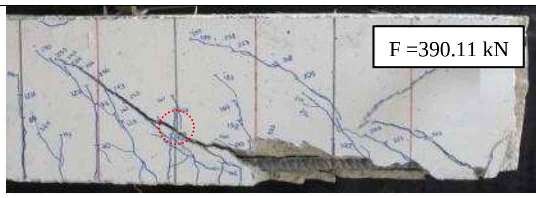
S300.90/ E300.45 (A.6, B.6)		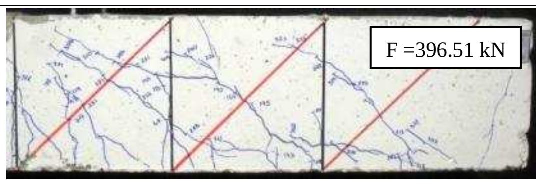
S225.90 (A.7)	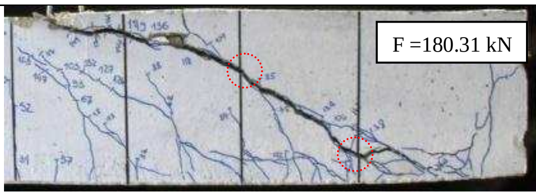	
S225.90/ E225.90 (A.8)	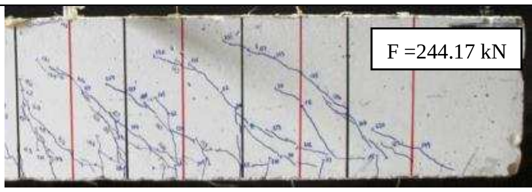	

Figure 17 – Crack pattern (the circule represents the zone where the steel stirrup has ruptured)

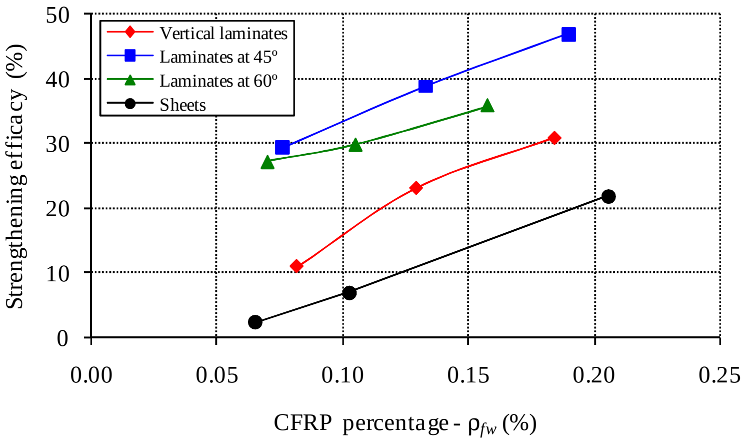

Figure 18 – Strengthening efficacy ($\Delta F_{max}/F_{max}^{2S\text{-}R}$) *vs* CFRP percentage (ρ_{fw}) (Dias and Barros 2012)